Supporting Information

Synergistic Computational-Experimental Approach to Improve Ionene Polymer-Based Functional Hydrogels

Content List

1. Chemicals and reagents

All chemicals used in this work, including reactants **4**–**7** and **11** (Scheme S1), were of analytical grade, purchased from commercial suppliers (Sigma Aldrich, TCI Europe) and used as received without any further purification. SWNTs with an average diameter of 0.7–1.3 nm were purchased from Sigma Aldrich. Double distilled water, additionally purified by a Milli-pore apparatus was used for preparing the hydrogels.

2. Materials characterization[i]

2.1. Monomers and ionene polymers

a) TLC analyses were performed using fluorescent-indicating plates (aluminum sheets precoated with silica gel 60 F_{254}, thickness 0.2 mm, Merck), and visualization achieved by UV light (λ_{max} = 254 nm) and staining with phosphomolybdic acid and/or iodine.

b) ^{1}H- and ^{13}C-NMR spectra were recorded at 25 ºC on Bruker Avance 300 or 400 MHz spectrometers. Chemical shifts are denoted in δ (ppm) relative to tetramethylsilane (TMS: δ = 0) as internal standard or relative to residual solvent peaks. Coupling constants, *J*, are given in Hertz. The following standard abbreviations are used for characterization of ^{1}H-NMR signals: s = singlet, d = doublet, t = triplet, m = multiplet. Estimated error of reported values: 0.01 ppm (δ, ^{1}H-NMR), 0.1 ppm (δ, ^{13}C-NMR), 0.1 Hz (*J*, coupling constant).

c) Elemental analyses were recorded on a Heraeus CHN elemental analyzer.

d) SEC data were obtained using a YL GPC instrument equipped with a refractive index detector. The temperature of column oven was maintained at 50–60 ºC. DMF including 30 mM of LiTFSA was used as eluent, and the flue rate maintained at 0.5 mL min^{-1}. Solutions of the samples were filtered through 0.2 μm filters before injection into the 10 μm columns. Molecular weights of ionenes were calibrated using poly(methyl methacrylate) standards.

We would like to emphasize the remarkable difficulties that we experienced to achieve batch-to-batch reproducible molecular weight distributions with this type of ionenes made via step-growth polymerizations, at least in our hands. As we could obtain reproducible NMR data in randomized experiments, such problematic is likely due to a) very strong interactions with the columns even after

anion exchange; b) fractionation in the purification process; c) sample exclusion within the column; and/or d) difference of reactivity between monomers and their polymer chains.[ii]

e) TGA/DSC/DTA measurements were carried out under nitrogen (flow = 100 mL min^{-1}) on a SDT Q600 TA instrument. The samples were placed into Pt crucibles and measured with the following program heating rate: (1) Equilibration step for 30 min @ 30 ºC; (2) heating profile from 30 ºC to 800 ºC @ 10 ºC/min; (3) isotherm step for 15 min @ 800 ºC. For checking reproducibility, TGA spectra were also carried out for different batches of samples using a Perkin Elmer Thermographic TGA-7 instrument.

2.2. Hydrogels and composites

a) FT-IR spectra were recorded using a Diamond ATR (attenuated total reflection) accessory (Golden Gate), in a VARIAN 1000 FT-IR (Scimitar™ Series) or in a Nicolet Avatar 360 FT-IR spectrophotometer.

b) UV-Vis-NIR spectra were recorded on a Jasco V-670 spectrophotometer using quartz cuvettes (path length, 1 cm).

c) T_{gel} values were determined by the inverse flow method[iii] (the seal vial containing the hydrogel or the hybrid was hung horizontally into an oil bath, which was heated up at 1 ºC min^{-1}). Herein, the temperature at which the gel started to break was defined as T_{gel}. Each measurement was made at least by duplicate and the average value reported. T_{gel} values were found almost unaltered within a difference of 1–2 ºC after several heating-cooling cycles.

d) CGC values were estimated by continuously adding aliquots of solvent (0.02–0.1 mL) into vials containing the corresponding ionene polymer and performing a typical heating-cooling protocol for gel-formation until no gelation was observed. The starting point for CGC determinations was 200 mg/mL.

e) Oscillatory rheology was performed with an AR 2000 Advanced rheometer (TA Instruments) equipped with a Julabo C cooling system. A 1000 μm gap setting and a torque setting of 40,000 dynes/cm^2 at 25 ºC were used for the measurements in a plain-plate (20 mm, stainless steel). The data were found to be highly reproducible for independent batches. The following experiments were carried out for each sample, using 2 mL total gel volume: a) Dynamic strain sweep (DSS): variation of G' and G'' with strain (from 0.01 to 100%); b) dynamic frequency sweep (DFS): variation of G' and G'' with

frequency (from 0.1 to 10 Hz at 0.1% strain); c) dynamic time sweep (DTS): variation of G' and G'' with time keeping the strain and frequency values constant and within the linear viscoelastic regime (strain = 0.1% strain; frequency = 1 Hz). Mechanical inertial effects of the measuring head was accounted by the software package to accurate evaluate the thixotropic nature of the materials through loop tests. For this, fixed rest time after sample loading and pre-shearing to equilibrium at different shear rates were routinely made in order to minimize prehistory effects.

Loop-tests involved the following steps: (1) Application of a low stress phase for 20 min at 0.1% oscillatory strain and 1Hz frequency as defined by DTS experiments (gel state, $G' > G''$), (2) increase of the shear strain rate until 4000% strain and 1 Hz frequency for 30 min to ensure gel-to-sol transition ($G' < G''$) and minimize inertial effects, and (3) relaxation for at least 240 min at the same conditions as for step (1) (recovered gel state, $G' > G''$).

f) Polarized optical microscopy (POM) was conducted using a Olympus BX51 microscope equipped with a Olympus DP12 digital camera at cross polarization of 90° using polarization filters. The samples were sandwiched between two cover glass slides for observation.

g) For electron microscopy, samples were observed with a (1) JEOL-2000 FXII transmission electron microscope (TEM, resolution = 0.28 nm) equipped with a CCD Gatan 694 digital camera and operating at 10 kV (accelerating voltage), and/or a (2) Carl Zeiss Merlin field emission scanning electron microscope (FE-SEM, resolution 0.8 nm) equipped with a digital camera and operating at 5 kV (accelerating voltage) and 10 μA (emission current). The aspect ratio of a fibre is defined as the ratio of its length to its width.

For TEM imaging, 10 μL of the hydrogel suspension was allowed to adsorb for 30 s onto carbon-coated grids (300 mesh, from TED PELLA, Inc.). After the adsorption, the excess solvent was removed by touching the edges with a small piece of filter paper (Whatman). The specimens were then dried overnight in a desecator at low pressure and RT. Patches of the gel were first searched to be sure that the observed structures originate from the gel. Micrographs were taken from structures at the periphery of the patches where the fibers were deposited in a layer thin enough to be observed by TEM. The large size of the sheet structures made negative staining unnecessary. For FE-SEM visualization, samples were prepared by the freeze-drying (FD) method:[iv] An eppendorf tube containing the corresponding hydrogel (100–200 μL) was frozen in liquid nitrogen or dry ice/acetone and the solvent immediately

evaporated under reduced pressure (0.6 mmHg) for 2 days at RT. A fibrous solid was obtained, which was placed on top of a tin plate and shielded by Pt (40 mA during 30 s (film thickness = 5 nm).

3. Materials synthesis

3.1. Procedure for the synthesis of monomers

To a stirred solution of the corresponding diaminobenzene **4**, **5** or **6** (500 mg, 4.55 mmol) and Et_3N (1.59 mL, 11.4 mmol) in CH_2Cl_2 (20 mL) at 0 ºC was added dropwise a solution of 4-(chloromethyl)benzoyl chloride (**7**) (1.75 g, 9.09 mmol) in CH_2Cl_2 (20 mL) via a pressure-compensated addition funnel. The reaction mixture was allowed to warm to RT and stir for 0.5–2 h (Scheme S1), after which time TLC analysis showed full conversion of the starting materials. The organic phase was washed with H_2O (2 × 15 mL) and brine (2 × 15 mL), dried over anhydrous Na_2SO_4, filtered, and concentrated via a rotary evaporator. The solid residue thus obtained was recrystallized from CH_2Cl_2/pentane, affording the desired bifunctional monomers (**8**, **9** or **10**, respectively**)** as crystalline solids. Monomer **8**: 96% yield (1.81 g, 4.37 mmol), white crystalline solid. Monomer **9**: 87% yield (1.64 g, 3.96 mmol), white slight brownish solid. Monomer **10**: 91% yield (1.71 g, 4.14 mmol), off-white solid. The corresponding spectroscopic data matched those reported in the literature for **8**,[v] **9**[vi] and **10**.[vii]

^{1}H-NMR (DMSO-d_6, 300 MHz) for **8**: δ (ppm) = 10.08 (s, 2H), 7.96 (d, J = 8.2 Hz, 4H), 7.67 (dd, J = 6.0, 3.6 Hz, 2H), 7.58 (d, J = 8.3 Hz, 4H), 7.30 (dd, J = 6.0, 3.5 Hz, 2H), 4.83 (s, 4H). ^{13}C-NMR (DMSO-d_6, 75 MHz) for **8**: ^{13}C: δ (ppm) = 164.92, 141.22, 133.97, 131.19, 128.83, 127.81, 125.80, 125.51, 45.23.

^{1}H-NMR (DMSO-d_6, 300 MHz) for **9**: δ (ppm) = 10.36 (s, 2H), 8.33 (t, J = 1.9 Hz, 1H), 7.98 (d, J = 8.3 Hz, 4H), 7.59 (d, J = 8.3 Hz, 4H), 7.51 (dd, J ^{13}C: δ (ppm) = 165.02, 140.92, 139.16, 134.66, 128.66, 128.52, 127.98, 116.02, 112.80, 45.33. ^{13}C-NMR (DMSO-d_6, 75 MHz) for **9**: δ (ppm) = 165.02, 140.92, 139.16, 134.66, 128.66, 128.52, 127.98, 116.02, 112.80, 45.33.

^{1}H-NMR (DMSO-d_6, 300 MHz) for **10**: δ (ppm) = 10.28 (s, 2H), 7.97 (d, J = 8.3 Hz, 4H), 7.76 (s, 4H), 7.59 (d, J = 8.4 Hz, 4H), 4.85 (s, 4H). ^{13}C-NMR (DMSO-d_6, 75 MHz) for **10**: δ (ppm) = 164.66, 140.87, 134.75, 131.13, 128.69, 127.89, 121.09, 120.55, 45.33.

It should be noted that, in contrast to bromides, the reactivity of ordinary dichlorides is generally too low to allow a Menshutkin reaction to proceed to reasonable conversions, and hence to achieve sufficient molar masses of the expected ionenes. However, the lower polarizability and leaving group ability of the dichlorides can be overcome by using activated analogs such as **7**.

3.2. Procedure for the synthesis of ionene polymers via co-polymerization of dielectrophilic and dinucleophilic monomers[viii]

To a stirred solution of the corresponding **8**, **9** or **10** (0.82 g, 2.00 mmol) in DMF (15, 45 or 25 mL, respectively) at 80 °C was added 1,4-diazabicyclo[2.2.2]octane (DABCO) **11** (0.22 g, 2.00 mmol) in one portion. The reaction mixture was stirred at 80 °C for 2–3 days (Scheme S1), after which time TLC analysis showed full conversion of the starting materials. The mixture was cooled down to RT and the precipitated polymers (**1**, **2** or **3**, respectively) thus obtained were isolated by filtration, washed subsequently with DMF, CH_3CN and CH_2Cl_2, and finally dried under vacuum. Ionene **1**: 98% yield (1.15 g, 1.96 mmol), white solid. Ionene **2**: 69% yield (0.81 g, 1.38 mmol), off-white slight brownish solid. Ionene **3**: 90% yield (1.08 g, 1.80 mmol), off-white solid. Spectroscopic data matched those reported in the literature for **3**.[ix]

^{1}H-NMR (D_2O, 300 MHz) for **1**: δ (ppm) = 7.86 – 7.26 (m, 6H), 4.54 – 4.18 (m, J = 6.7 Hz, 1H), 3.93 – 3.66 (m, J = 28.2, 12.4 Hz, 4H), 3.42 – 3.18 (m, J = 15.8, 6.9 Hz, 2H), 3.13 – 2.94 (m, J = 12.7, 6.7 Hz, 2H).

^{1}H-NMR (D_2O, 300 MHz) for **2**: δ (ppm) = 8.00 – 7.18 (m, 6H), 4.44 (s, 1H), 3.91 (s, 4H), 3.34 (d, J = 6.6 Hz, 2H), 3.05 (d, J = 6.2 Hz, 2H).

^{1}H-NMR (D_2O, 300 MHz) for **3**: δ (ppm) = 7.88 (s, 2 H), 7.72 – 7.39 (m, 4H), 4.67 – 4.23 (m, 1H), 3.82 (bs, 4H), 3.33 (bs, 2H), 3.05 (bs, 2H).

*3.3. Procedure for the preparation of ionene (**1–3**)·**TFSA** via anion exchange*

A solution of lithium bis(trifluoromethanesulfonyl)amide, LiTFSA, (1.0 g) in water (5–10 mL) was added to a solution of the corresponding ionene **1**–**3** (0.10 g) in water (20–100 mL) at 90 ºC and the mixture stirred for 5–30 min to afford the ionene·TFSA as precipitates. The polymers were isolated by

filtration, washing and drying under vacuum. Ionene **1·TFSA**: 88% yield (0.17 g), white solid. Ionene **2·TFSA**: 47% yield (0.09 g), white solid. Ionene **3·TFSA**: 82% yield (0.16 g), off-white solid.

^{1}H-NMR (DMSO-d_6, 300 MHz) for **1·TFSA**: δ (ppm) = 10.15 (s, 1H), 8.07 (d, J = 7.9 Hz, 2H), 7.69 – 7.51 (m, 3H), 7.33 (s, 1H), 4.77 (s, 2H), 3.79 (s, 4H), 3.28 (bs, 1H), 3.02 (bs, 1H).

^{1}H-NMR (DMSO-d_6, 300 MHz) for **2·TFSA**: δ (ppm) = 10.43 (d, J = 5.8 Hz, 2H), 8.42 (s, 1H), 8.25 – 7.98 (m, 2H), 7.67 (d, J = 6.3 Hz, 4H), 7.49 (t, J = 7.9 Hz, 2H), 7.35 (t, J = 8.0 Hz, 1H), 4.83 (s, 2H), 3.85 (s, 8H), 3.30 (d, J = 7.7 Hz, 2H), 3.03 (d, J = 6.9 Hz, 2H).

^{1}H-NMR (DMSO-d_6, 300 MHz) for **3·TFSA**: δ (ppm) = 10.37 (d, J = 4.7 Hz, 1H), 8.12 (q, J = 11.2 Hz, 2H), 7.75 (d, J = 11.3 Hz, 2H), 7.64 (dd, J = 15.5, 8.2 Hz, 2H), 4.70 (d, J = 74.8 Hz, 2H), 3.84 (s, 4H), 3.31-3.29 (m, 1H), 3.05 (m, 1H).

3.3. Procedure for the preparation of hydrogels and composites

Typically, a weighted amount of the corresponding polymer **1**, **2** or **3** and Milli-Q water (1 mL) were placed into a screw-capped glass vial (4 cm length × 1 cm diameter) and gently heated with a heat gun until the solid material was completely dissolved. The resulting isotropic solution was then spontaneously cooled down to RT. No control over temperature rate during the heating-cooling process was applied. The material was preliminary classified as "gel" if it did not exhibit gravitational flow upon turning the vial upside-down at RT. The state was further confirmed by rheological measurements. Physical incorporation of SWCNT into the corresponding hydrogels was carried out as following: Typically, a specific amount of SWCNT was placed on top of the suitable hydrogel (1 mL), capped, and subjected to homogeneous dispersion upon sonication for 60 min at RT using a VWR ultrasonic cleaner (USC200TH) at 45 kHz and 120 W. The resulting solution was left undisturbed for at least 12 h at RT to allow complete reconstitution of the gel phase and formation of stable composites.

4. Computational studies

4.1. Simulated models

Simplified molecular systems for **1**, **2** and **3**-based hydrogels were constructed considering two polymer chains with 6 repeat units each one, which were placed relatively close to facilitate the formation of specific interactions. A chloride counter-ion was added next to each charged group (i.e., two positive

charges per repeat unit), which represented a total of 24 chloride counter-ions per molecular system. Each molecular system (i.e., the two polymer chains with six repeat units and the corresponding counter-ions) was placed in the centre of an orthorhombic box filled with water molecules that were previously equilibrated at 1 atm and 298 K. Those solvent molecules overlapping either a polymer atom or a chloride ion were removed. The dimensions of the simulation box, the final number of water molecules contained in the simulation box and the total number of explicit particles considered in the simulation for each molecular model are given next: Molecular system **1**: simulation box ($Å^3$) = 149 × 130 × 130; number of water molecules = 77958; total number of explicit particles = 234708. Molecular system **2**: simulation box ($Å^3$) = 167 × 145 × 145; number of water molecules = 110448; total number of explicit particles = 332178. Molecular system **3**: simulation box ($Å^3$) = 167 × 145 × 145; number of water molecules = 108717; total number of explicit particles = 326985. Additional simulations were carried out using an extended model of **2**, denoted **2e**, which was made of four polymer chains with 6 repeat units each one and 48 chloride counter-ions. The characteristics of such model, which was constructed using the procedure discussed above for **1**–**3**, are: simulation box ($Å^3$) = 150 × 140 × 150; number of water molecules = 98498; total number of explicit particles = 297158. Finally, simulations on **1w** and **2w**, which contained two polymer chains with 8 repeat units each one, were carried out considering 103945 (simulation box= 155 × 135 × 135 $Å^3$) and 147264 (simulation box= 165 × 145 × 145 $Å^3$) explicit water molecules, respectively.

4.2. Force field details

All parameters were extrapolated from AMBER03 libraries[x] with exception of partial charges of each hydrogel repeat unit. Water molecules were represented by the TIP3 model.[xi] Van der Waals interactions were computed using an atom pair cut-off distance of 14.0 Å. In order to avoid discontinuities in the potential energy function, non-bonding energy terms were forced to slowly converge to zero, by applying a smoothing factor from a distance of 12.0 Å. Electrostatic interactions were extensively computed by means of Ewald summations. The real space term was defined by the van der Waals cutoff, while the reciprocal space was computed by interpolation into an infinite grid of points (particle mesh Ewald) with maximum space grid points being 1.0 Å.[xii] Bond lengths were constrained using the *SHAKE* algorithm[xiii] with a numerical integration step of 2 fs. A set of partial charges was explicitly derived for the repeat unit of each studied hydrogel. Partial charges were obtained by fitting the rigorously defined quantum mechanical molecular electrostatic potential (MEP)

to the Coulombic electrostatic potential. For consistency with the AMBER force field, the MEP was computed at the HF/6-31G(d) level.[xiv] Atomic electrostatic parameters were derived by fitting the quantum mechanical MEP values into partial charges centered in the nuclei through a Levenberg–Marquardt nonlinear optimization procedure. Quantum mechanics calculations were performed with Gaussian 03 program.[xv]

4.3. Computational details

All simulations were performed using NAMD 2.7 program.[xvi] Each system was submitted to 5000 steps of energy minimization using the Newton Raphson method. The minimized structure was the starting point of 300000 steps of NPT MD simulation, in which the water molecules were the only particles allowed to move until the density was equilibrated to around 1 $g \cdot cm^{-3}$. In this run temperature was kept constant using the Langevin method[xvii] with a damping coefficient of 0.5 ps^{-1} while the Berendesen barostast[xviii] was used to reach the proper density considering a pressure of 1 atm, relaxation time of 1 ps and a rescaling frequency of 0.01 ps. The resulting configuration was the starting point for 200000 steps of NPT MD simulation, in which all atoms of the system were allowed to be mobile. For this run and the following simulated periods, the pressure control was performed by means of the Nose–Hoover[xix] piston combined with the piston fluctuation control implemented for Langevin Dynamics[xx] for the temperature control. Pressure was kept at 1 atm, the oscillation period was set at 0.2 ps while the decay time was set at 0.06 ps. The piston temperature was set at the same value as the thermostat control, 298K, which used a damping coefficient of 1 ps^{-1}. The last snapshot of the latter run was the starting point of 5 ns of MD production time using identical conditions.

4.4. Density Functional Theory (DFT) calculations

DFT calculations were carried out considering models complexes of **1**, **2** and **3**. Each complex was formed by two fragments (subsystems), each one made with part of one monomer (n = 1 in Figure 2). Thus, positively charged six-membered rings were not considered in model complexes, subsystems being initially arranged to optimize intermolecular hydrogen bonding interactions (i.e., H···O distances of ~2.0 Å and ∠N–H···O angles as close as possible to 180º). Molecular geometries were optimized in the gas-phase using the M06L pure functional[xxi] combined with the 6-31+G(d,p) basis set.[xxii,xxiii] It should be mentioned that the M06L was found to be the most trustworthy DFT method in Gaussian09 to study non-covalently interacting systems.[xxiv] Interaction energies in the gas-phase (ΔE_i^{gp}) were

estimated as the difference between the total energy of the optimized complex (E_{AB}) and the energies of the isolated subsystems with the geometries obtained from the optimization of the complex:

$$\Delta E_i^{gp} = E_{AB} - E_{A(B)} - E_{B(A)} \quad (1)$$

where $E_{A(B)}$ and $E_{B(A)}$ refer to the energies of subsystems after correct the basis set superposition error (BSSE) using the counterpoise (CP) method.[xxv] The binding energies in the gas-phase (ΔE_b^{gp}), which takes into account geometrical changes associated to the formation of intermolecular interactions, were calculated as follows:

$$\Delta E_b^{gp} = E_{(AB)} - 2E_{A-i} \quad (2)$$

where $E_{(AB)}$ represents the two-body interaction energy corrected according to the counterpoise philosophy (Eqn 3) and $E_{A\text{-}i}$ is the energy obtained from the complete optimization of the isolated subsystem.

$$\Delta E_{(AB)} = E_A + E_B + E_{AB} - E_{A(B)} - E_{(A)B} \quad (3)$$

Environmental effects (here water) have been accounted for using the well-known Polarizable Continuum model (PCM).[xxvi] PCM calculations were performed in the framework of the DFT M06L/6-31+G(d,p) level using the standard protocol and considering the dielectric constant of water (ε= 78.4). The binding energy in solution was estimated as:

$$\Delta E_b^{wat} = \Delta E_b^{gp} + \Delta\Delta G_{wat,d} \quad (4)$$

where $\Delta\Delta G_{wat,d}$ is the difference between the free energy of solvation of the complex and the separated subsystems.

All DFT and PCM calculations were performed using the Gaussian09 program,[xv] applying default thresholds and algorithms.

Table S1. Interaction and binding energies in the gas-phase (ΔE_i^{gp} and ΔE_b^{gp}, respectively) and binding energies in aqueous solution (ΔE_b^{wat}) calculated for model complexes of **1-3** using M06L/6-31+G(d,p) and PCM-M06L/6-31+G(d,p) calculations.

Ionene	ΔE_i^{gp} (kcal/mol)	ΔE_b^{gp} (kcal/mol)	ΔE_b^{wat} (kcal/mol)
1	-27.8	-23.3	-11.3
2	-28.0	-24.0	-12.4
3	-21.1	-19.1	-9.4

Calculated interaction energies in the gas-phase (ΔE_i^{gp}) suggest that the strength of secondary intermolecular interactions is similar for **1** and **2**, while intermolecular hydrogen bonds and, especially, π-π interactions are clearly weaker for **3**. This behavior is fully consistent with the geometric parameters displayed in Figure S20. Incorporation of geometry relaxation effects through the estimation of ΔE_b^{gp} does not provoke major changes in these relative abilities to form intermolecular secondary interactions. However, as it was expected, the energy penalty associated to the geometry relaxation (ΔE_G) is lower for the compound with *N,N'*-(-*para*-phenylene)dibenzamide linkages (ΔE_G= 2.0 kcal/mol) than for those with *meta* and *ortho* architectures (ΔE_G= 4.0 and 4.5 kcal/mol, respectively). Finally, the binding energies calculated in water allow us to conclude that in solution the dimerization of **1** and **2** is also favored with respect to that of **3**.

It is worth noting that, although these calculations cannot be used to explain the gelation behavior of **1-3** from a quantitative point of view because of the model complexes, an important observation can be extracted from the energy values listed in Table S1 and the geometries displayed in Figure S20. The *N,N'*-(-*ortho*-phenylene)dibenzamide linkages of **1** are suitable to form a dense network of intra- and intermolecular secondary interactions (i.e. hydrogen bonds and, especially, π-π interactions), which is not possible for compounds with *N,N'*-(-*meta*-phenylene)dibenzamide and *N,N'*-(-*para*-phenylene)dibenzamide linkages. These feature combined with energy values listed in Table S1 suggests that the gelation ability observed for **1**, which is higher than that of **2**, may be enhanced by cooperative effects associated to such large network of interactions. Unfortunately, huge size of models required to get quantitative (DFT calculations) or even qualitative (MD simulations) information about the possible existence of such cooperative effects precludes a deeper analysis on this topic.

5. Additional schemes and figures

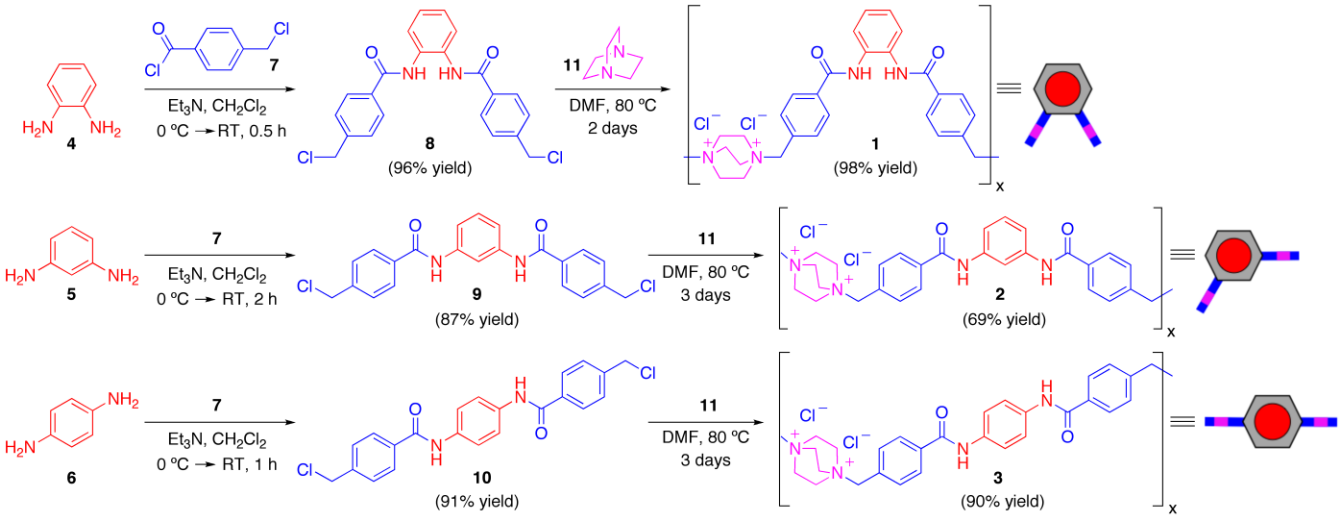

Scheme S1. Synthesis of DABCO-containing ionene polymers **1**–**3** with *N*,*N*'-(*x*-phenylene)dibenzamide linkages (*x* = *ortho*-/*meta*-/*para*-). Notes: a) Net dipole moment for each isomer: μ_r (*ortho*) = $\sqrt{(\mu_1^2 + \mu_2^2 + \mu_1\mu_2)}$; μ_r (*meta*) = $\sqrt{(\mu_1^2 + \mu_2^2 - \mu_1\mu_2)}$; μ_r (*para*) = $\sqrt{(\mu_2 - \mu_1)}$. b) Same results were obtained in the case of **1** upon either 2 days or 3 days of polymerization between **8** and **11**.

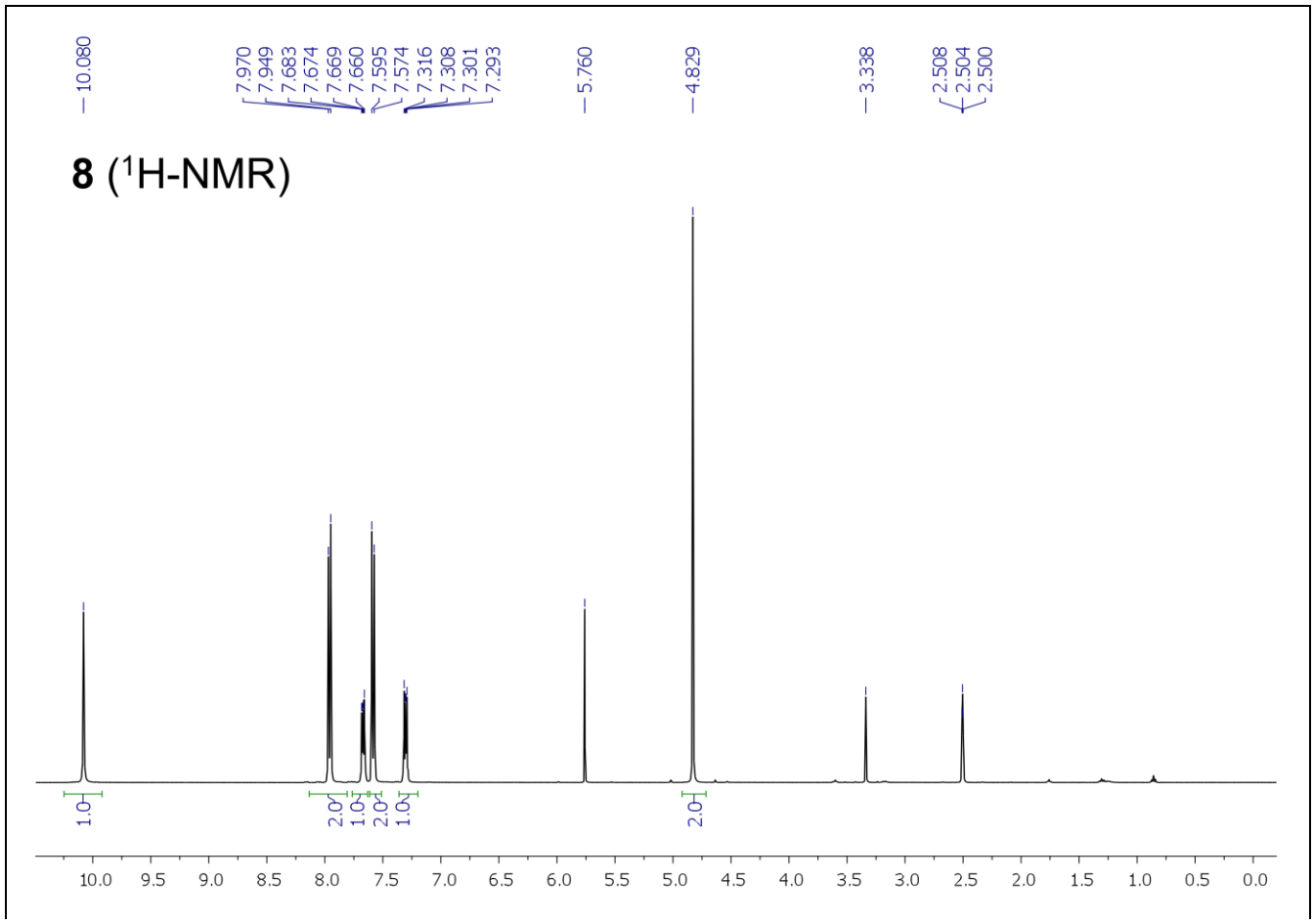
10.080
7.970
7.949
7.683
7.674
7.669
7.660
7.595
7.574
7.316
7.308
7.301
7.293
5.760
4.829
3.338
2.508
2.504
2.500
8 (1H-NMR)
1.0
2.0
1.0
2.0
1.0
2.0
10.0 9.5 9.0 8.5 8.0 7.5 7.0 6.5 6.0 5.5 5.0 4.5 4.0 3.5 3.0 2.5 2.0 1.5 1.0 0.5 0.0

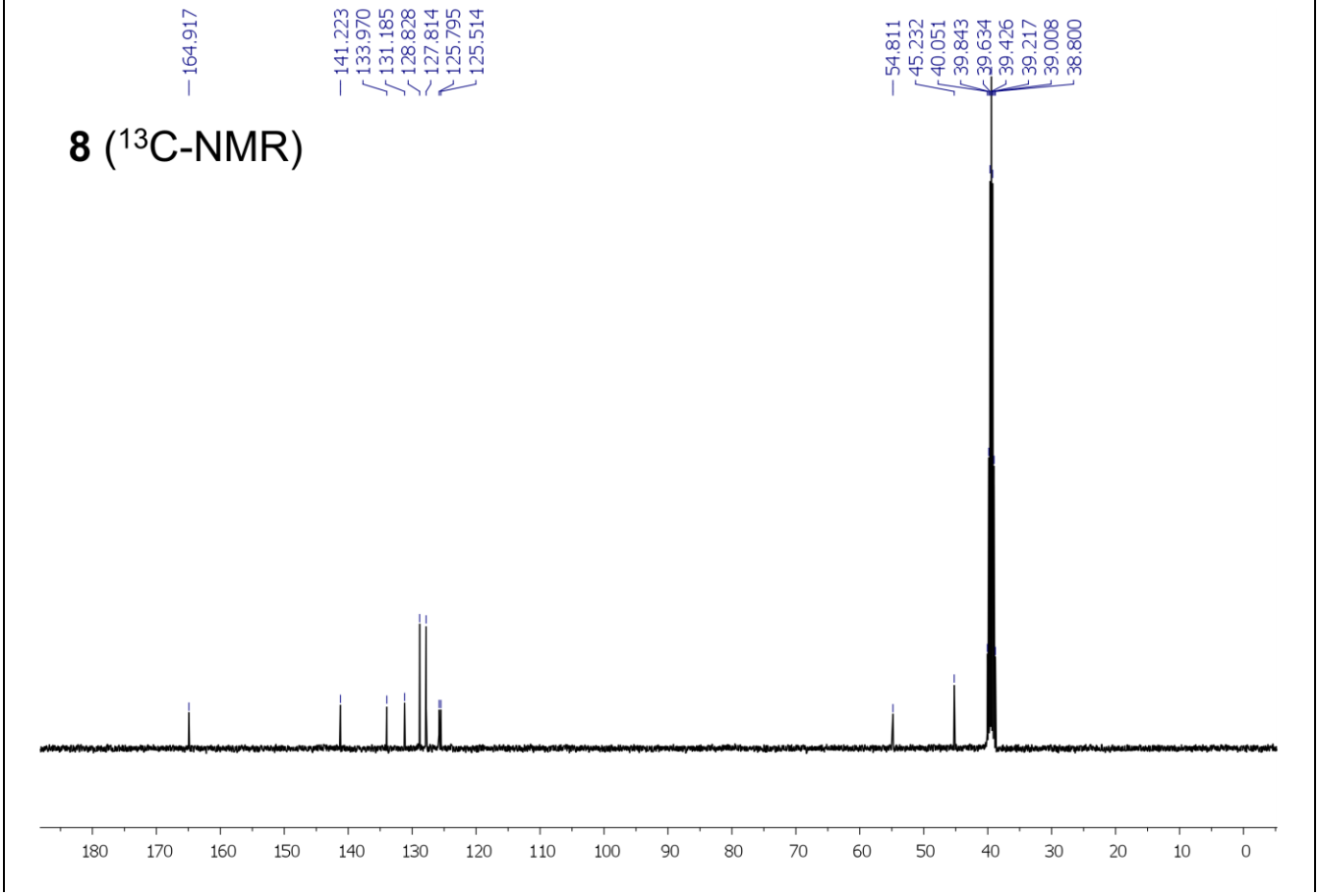
8 (13C-NMR)
164.917
141.223
133.970
131.185
128.828
127.814
125.795
125.514
54.811
45.232
40.051
39.843
39.634
39.426
39.217
39.008
38.800
180
170
160
150
140
130
120
110
100
90
80
70
60
50
40
30
20
10
0

9 (^{1}H-NMR)

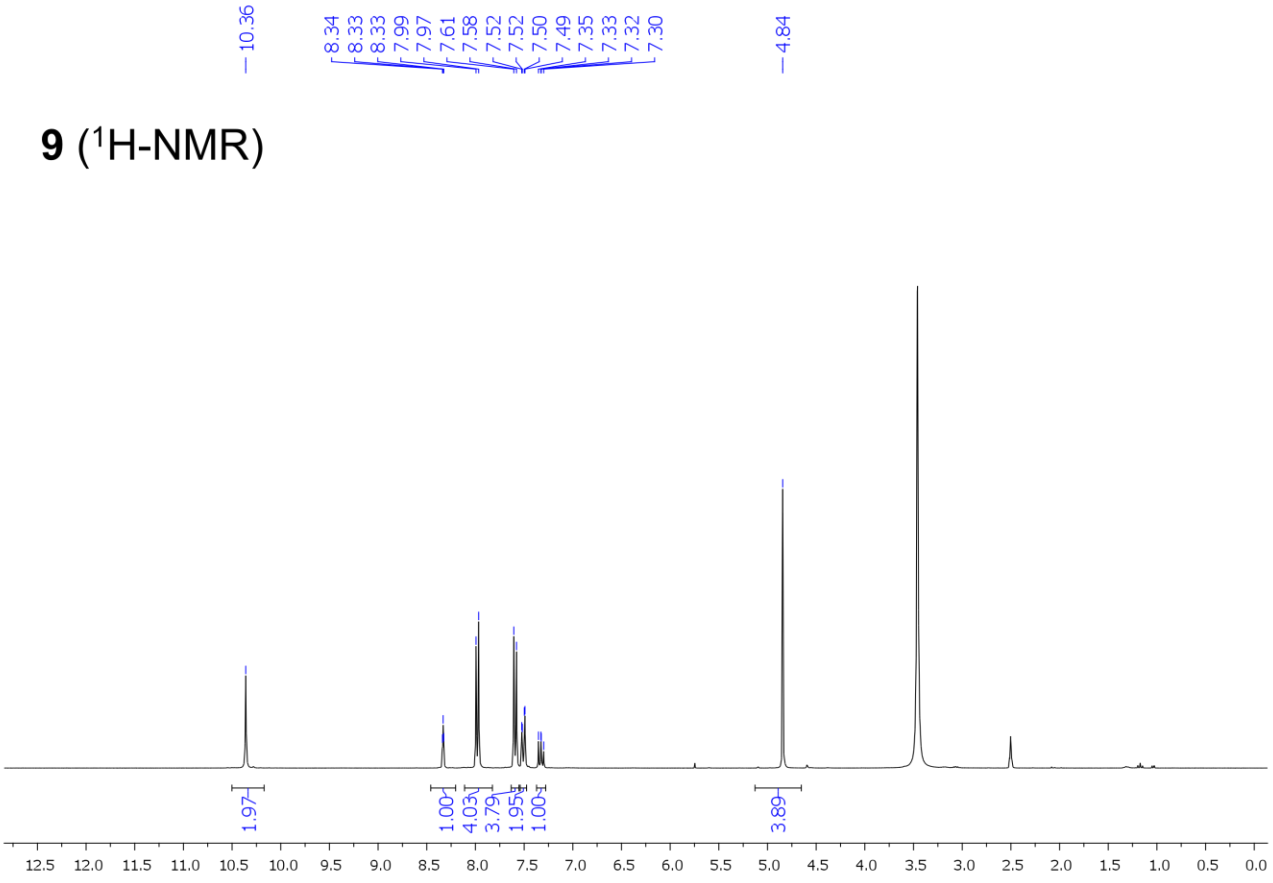
10.36
8.34
8.33
8.33
7.99
7.97
7.61
7.58
7.52
7.52
7.50
7.49
7.35
7.33
7.32
7.30
4.84
1.97
1.00
4.03
3.79
1.95
1.00
3.89
12.5 12.0 11.5 11.0 10.5 10.0 9.5 9.0 8.5 8.0 7.5 7.0 6.5 6.0 5.5 5.0 4.5 4.0 3.5 3.0 2.5 2.0 1.5 1.0 0.5 0.0

9 (^{13}C-NMR)

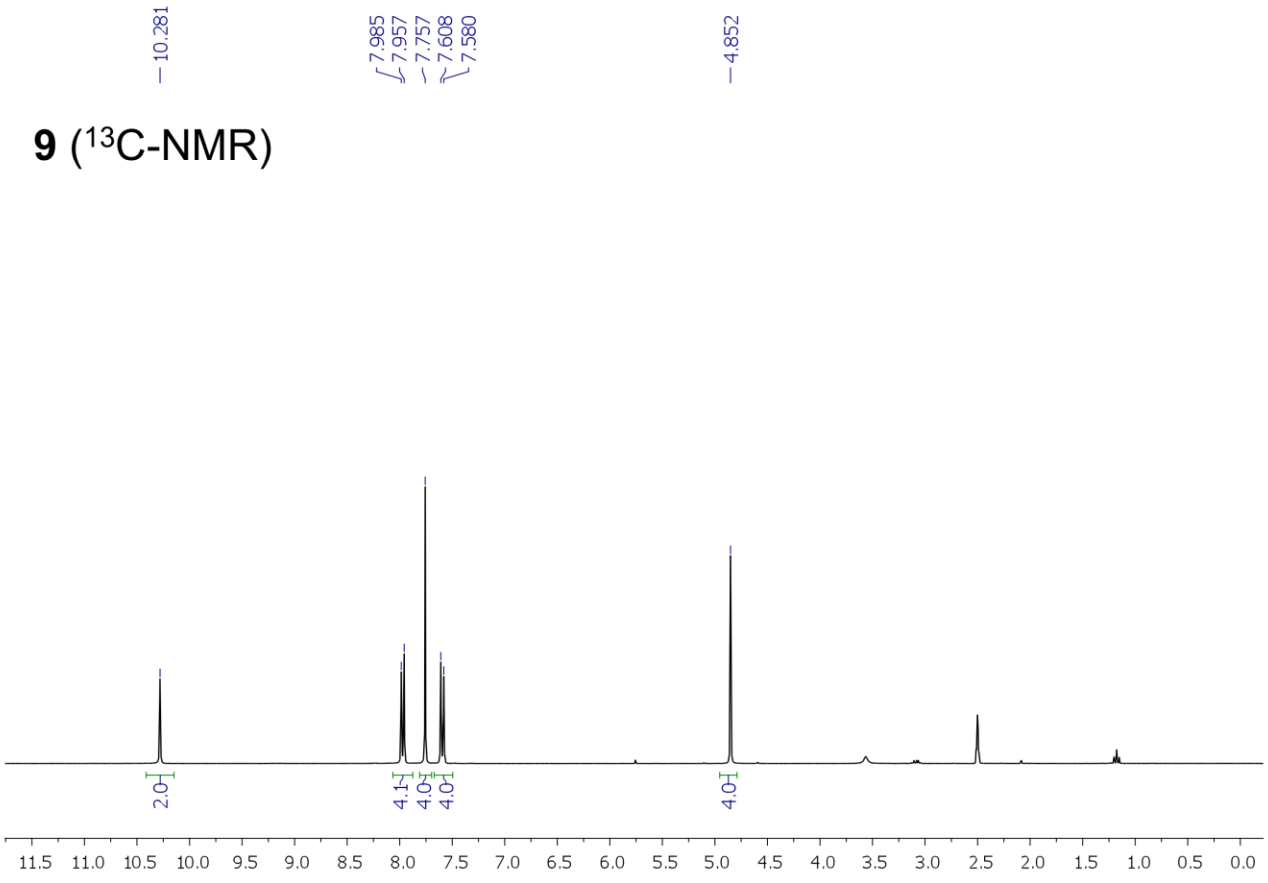
10.281
7.985
7.957
7.757
7.608
7.580
4.852
2.0
4.1
4.0
4.0
4.0
11.5 11.0 10.5 10.0 9.5 9.0 8.5 8.0 7.5 7.0 6.5 6.0 5.5 5.0 4.5 4.0 3.5 3.0 2.5 2.0 1.5 1.0 0.5 0.0

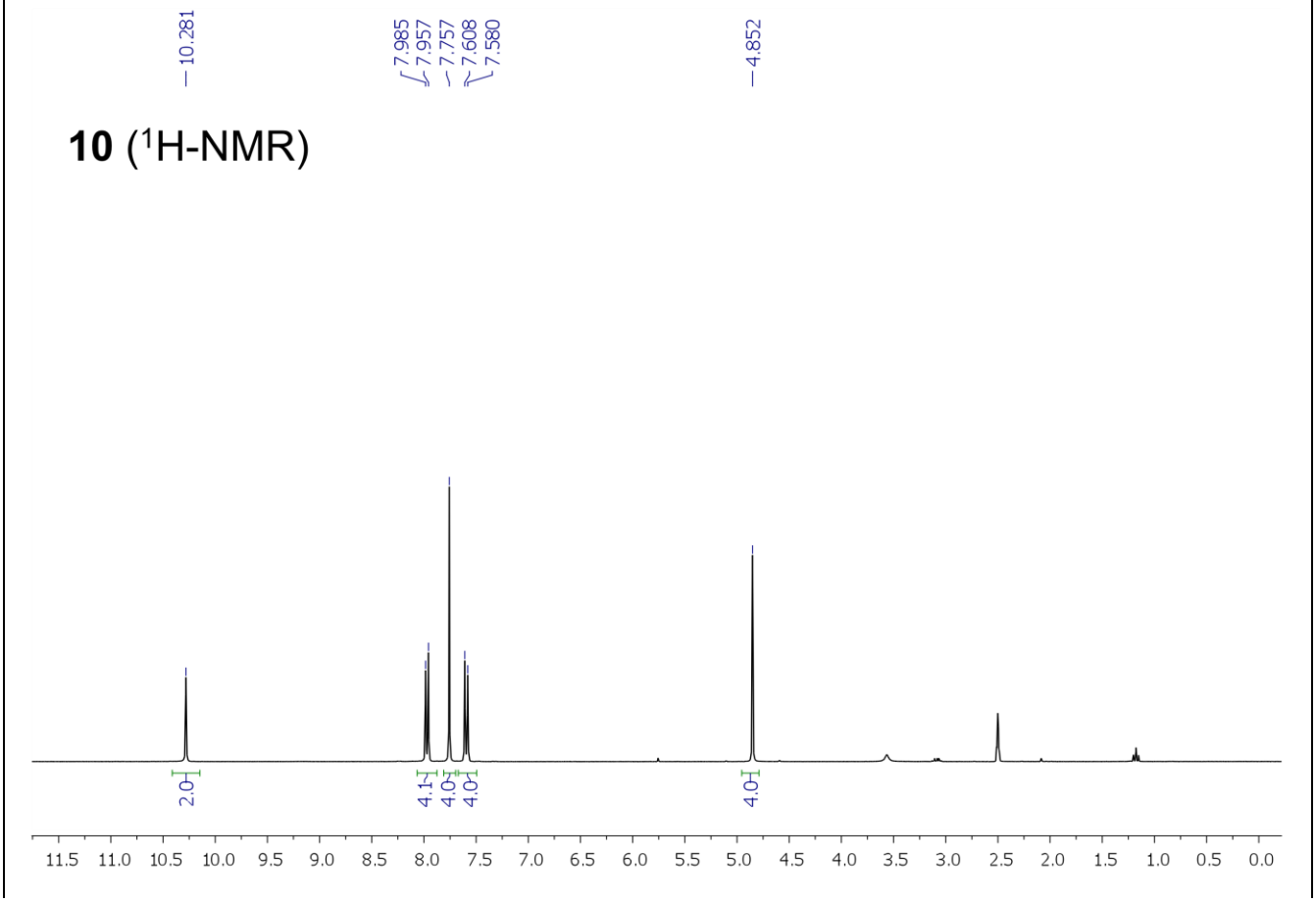
10.281
7.985
7.957
7.757
7.608
7.580
4.852
10 (1H-NMR)
2.0
4.1
4.0
4.0
4.0
11.5 11.0 10.5 10.0 9.5 9.0 8.5 8.0 7.5 7.0 6.5 6.0 5.5 5.0 4.5 4.0 3.5 3.0 2.5 2.0 1.5 1.0 0.5 0.0

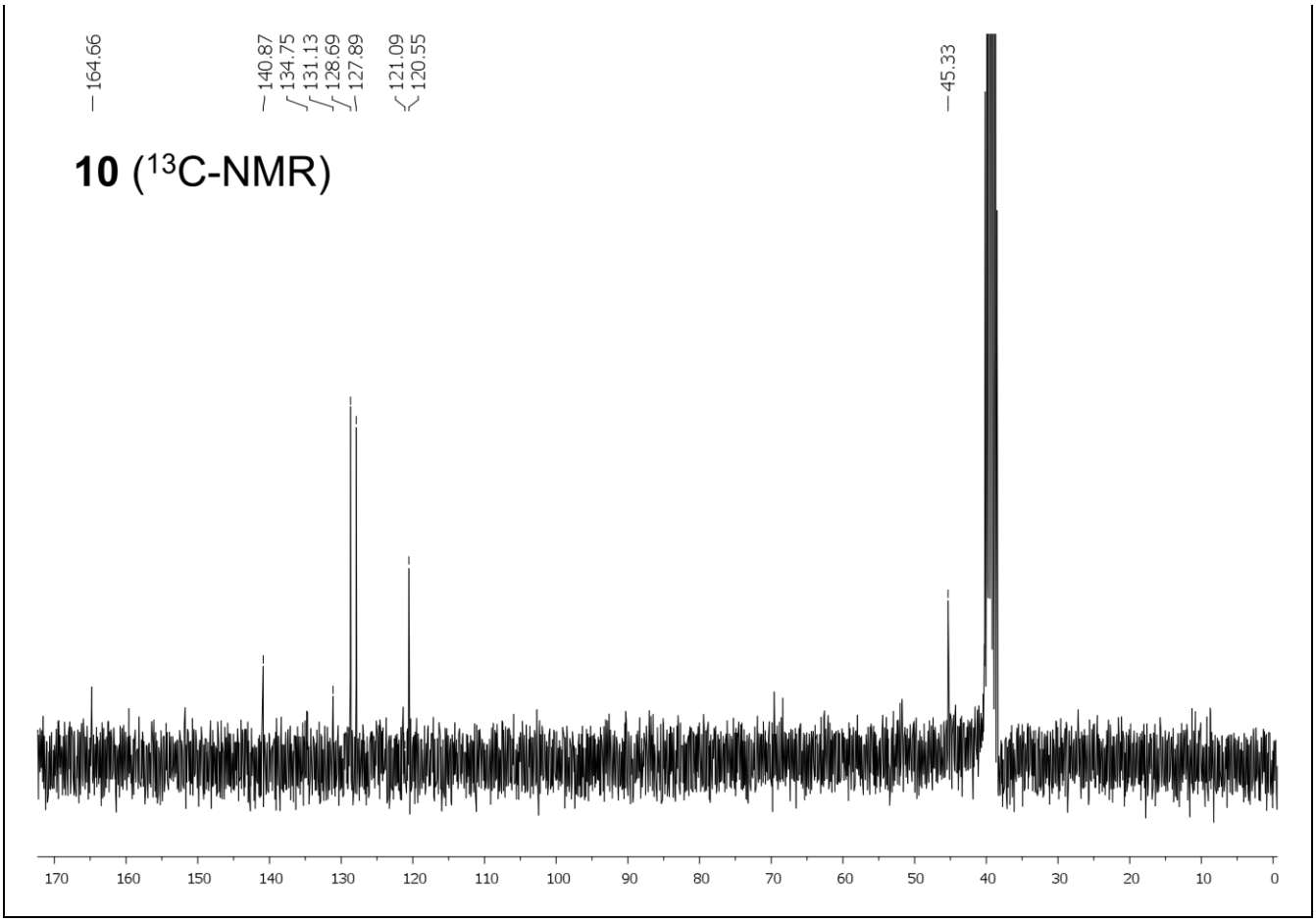

Figure S1. ^{1}H- (300 MHz) and ^{13}C-NMR (75 MHz) spectra of polymer precursors ionenes **8**–**10** in DMSO-d_6.

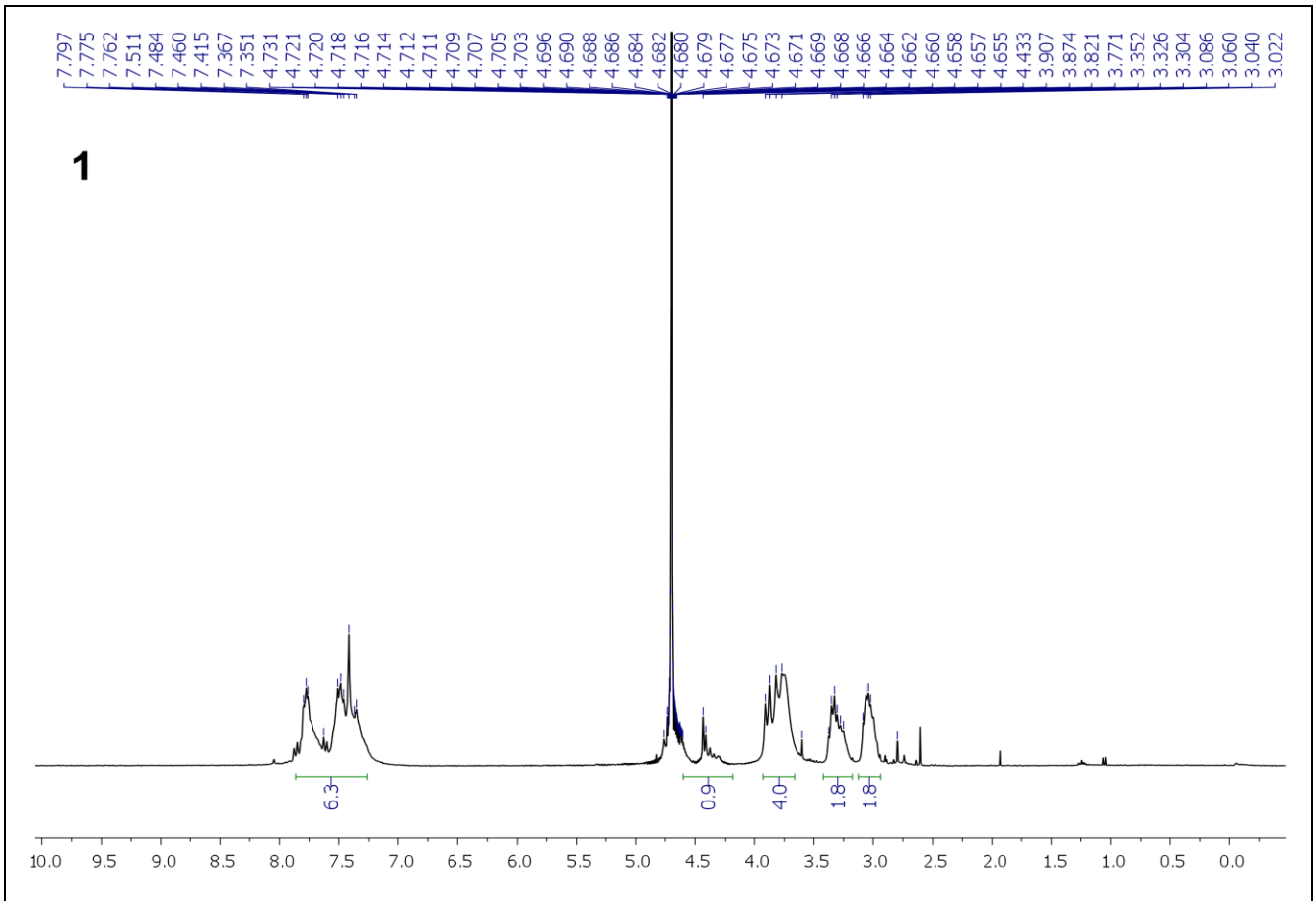
1
7.797
7.775
7.762
7.511
7.484
7.460
7.415
7.367
7.351
4.731
4.721
4.720
4.718
4.716
4.714
4.712
4.711
4.709
4.707
4.705
4.703
4.696
4.690
4.688
4.686
4.684
4.682
4.680
4.679
4.677
4.675
4.673
4.671
4.669
4.668
4.666
4.664
4.662
4.660
4.658
4.657
4.655
4.433
3.907
3.874
3.821
3.771
3.352
3.326
3.304
3.086
3.060
3.040
3.022
6.3
0.9
4.0
1.8
1.8
10.0
9.5
9.0
8.5
8.0
7.5
7.0
6.5
6.0
5.5
5.0
4.5
4.0
3.5
3.0
2.5
2.0
1.5
1.0
0.5
0.0

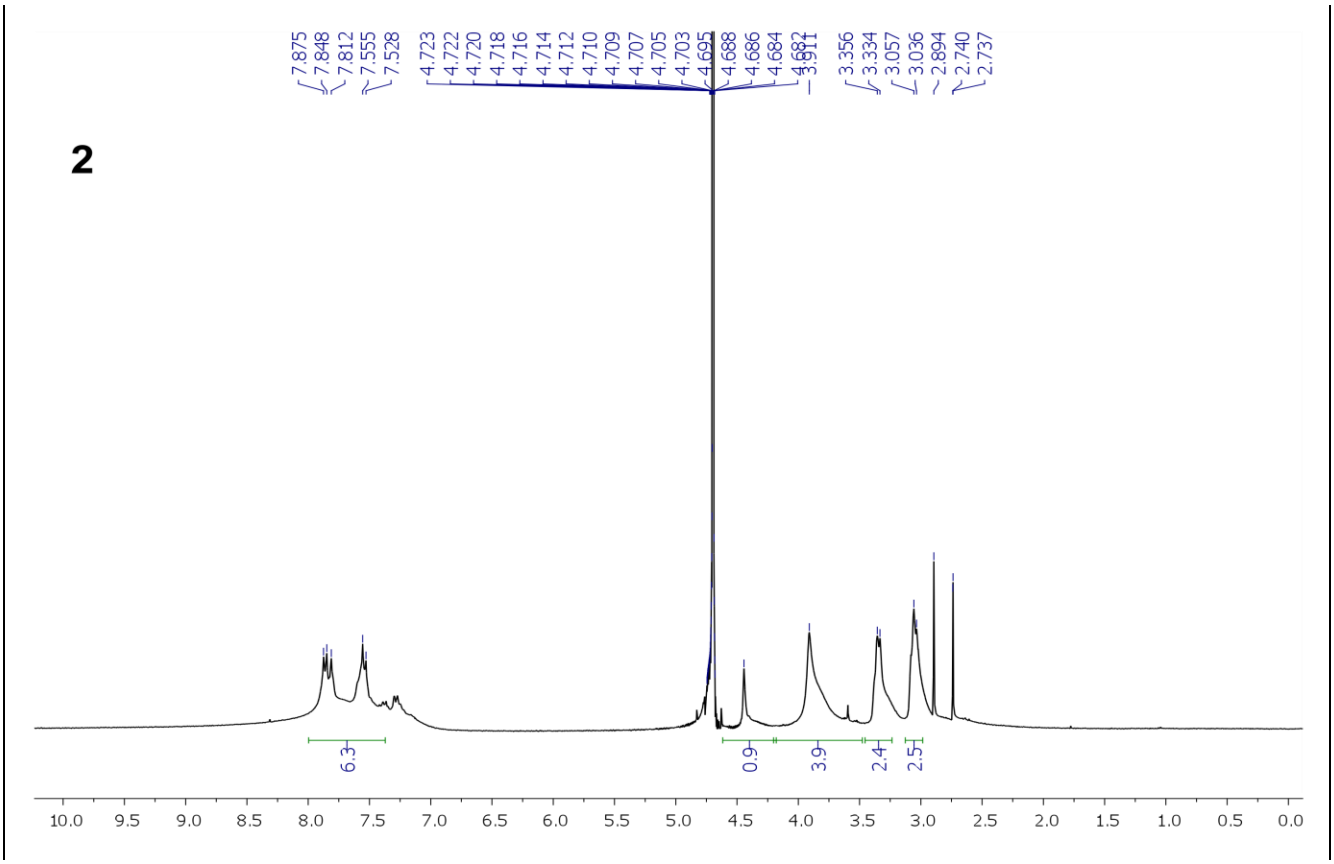
2
7.875
7.848
7.812
7.555
7.528
4.723
4.722
4.720
4.718
4.716
4.714
4.712
4.710
4.709
4.707
4.705
4.703
4.695
4.688
4.686
4.684
4.682
3.911
3.356
3.334
3.057
3.036
2.894
2.740
2.737
6.3
0.9
3.9
2.4
2.5
10.0
9.5
9.0
8.5
8.0
7.5
7.0
6.5
6.0
5.5
5.0
4.5
4.0
3.5
3.0
2.5
2.0
1.5
1.0
0.5
0.0

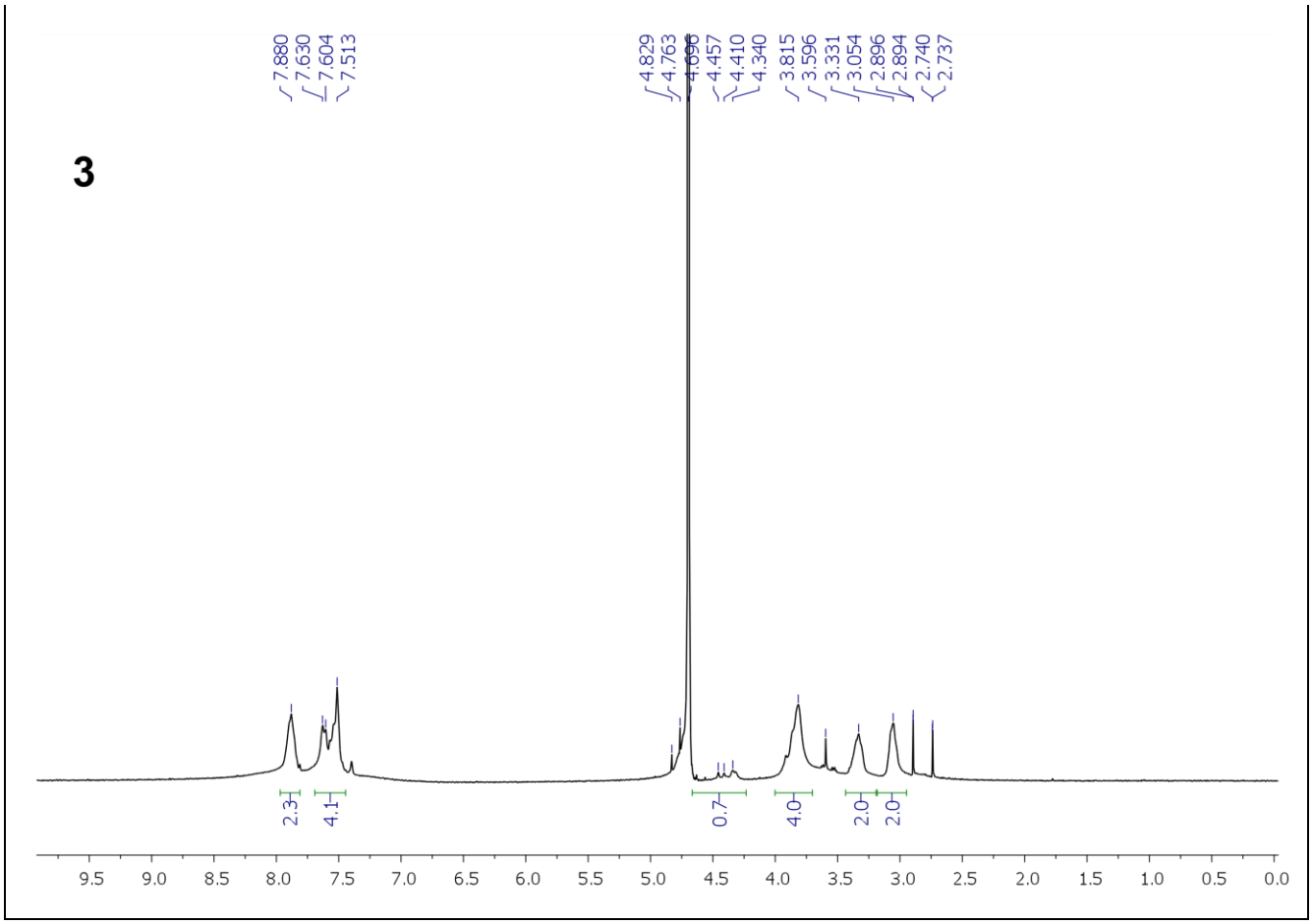

Figure S2. ^{1}H-NMR (300 MHz) spectra of ionenes **1**–**3** in D_2O.

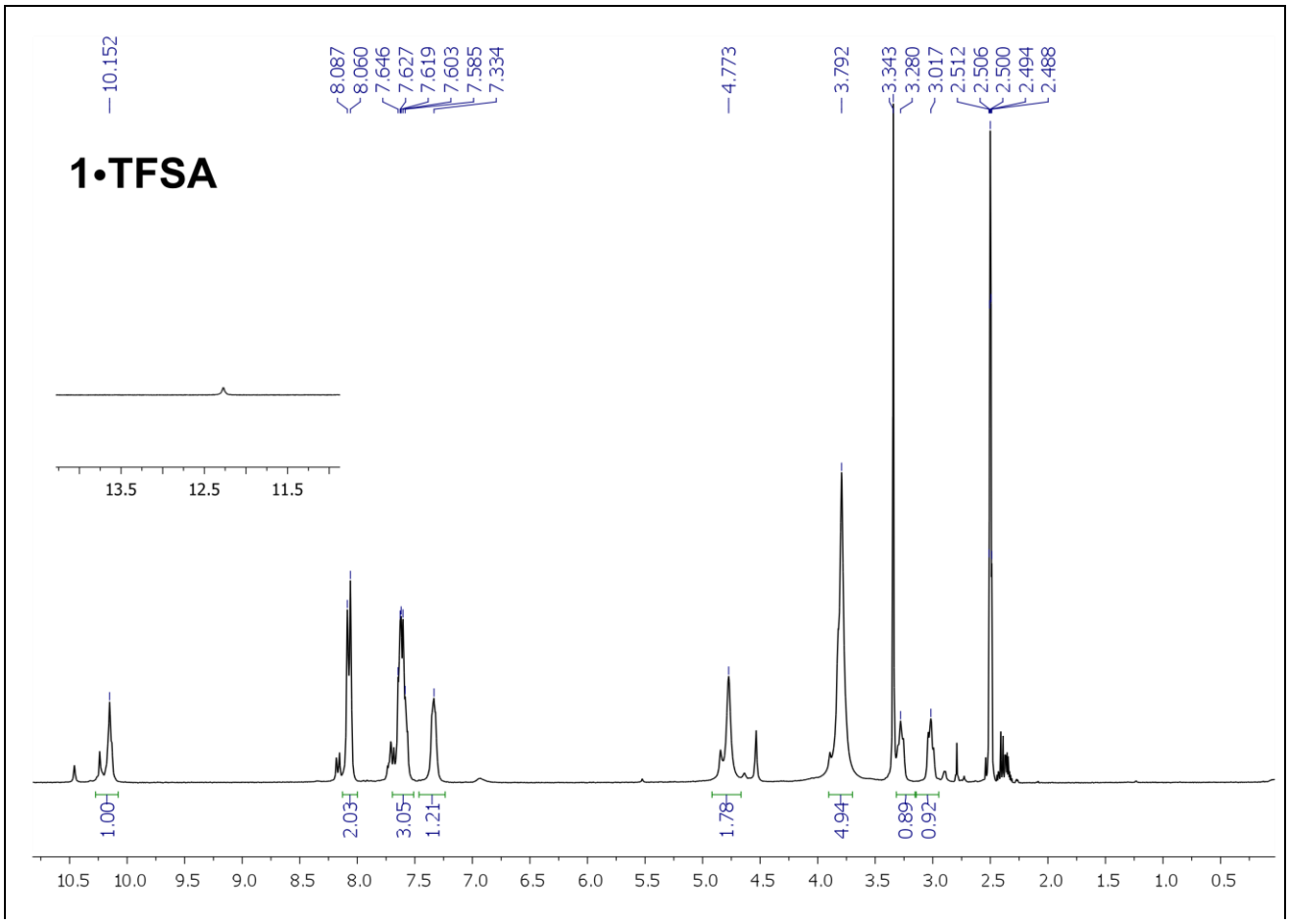
1•TFSA
10.152
8.087
8.060
7.646
7.627
7.619
7.603
7.585
7.334
4.773
3.792
3.343
3.280
3.017
2.512
2.506
2.500
2.494
2.488
13.5
12.5
11.5
1.00
2.03
3.05
1.21
1.78
4.94
0.89
0.92
10.5 10.0 9.5 9.0 8.5 8.0 7.5 7.0 6.5 6.0 5.5 5.0 4.5 4.0 3.5 3.0 2.5 2.0 1.5 1.0 0.5

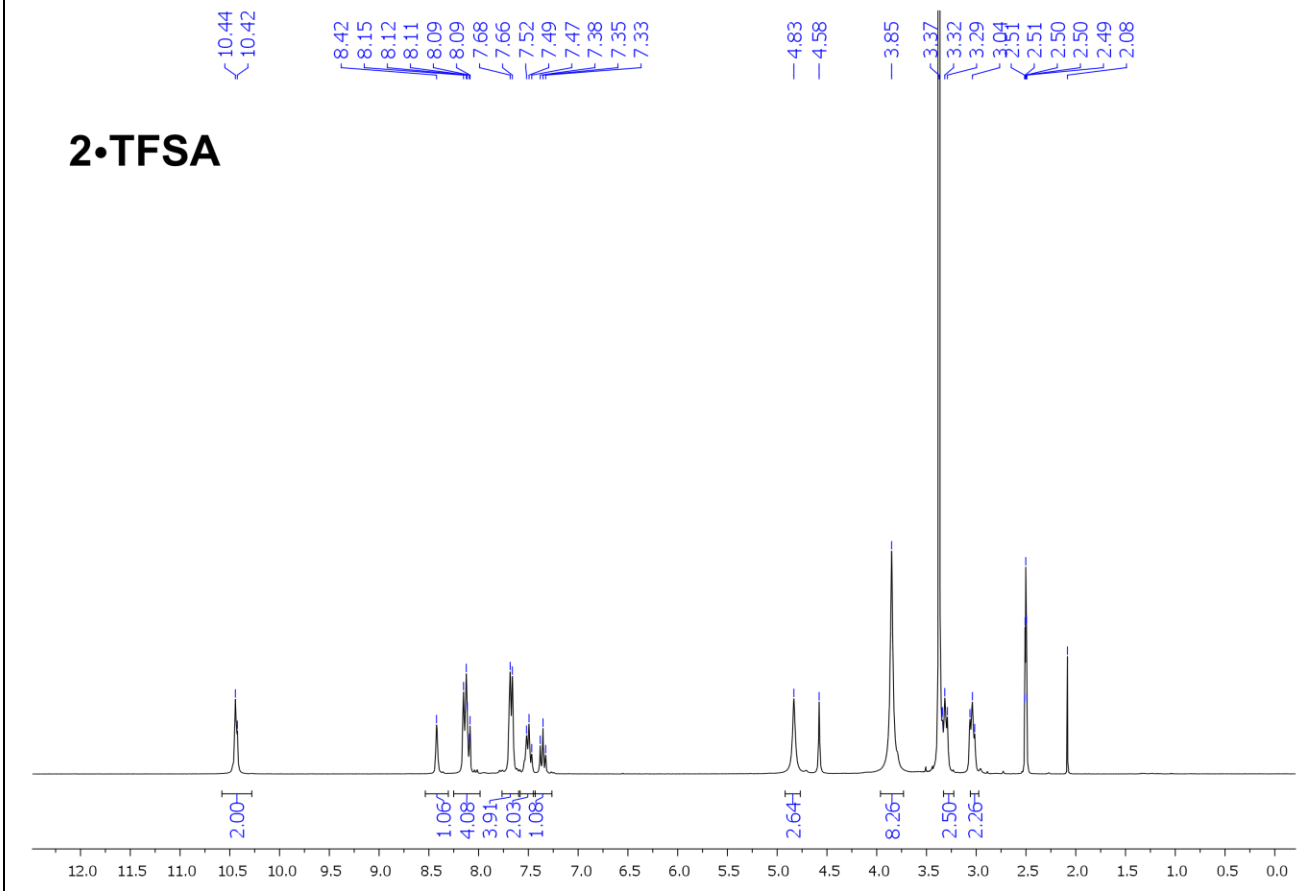
2•TFSA
10.44
10.42
8.42
8.15
8.12
8.11
8.09
8.09
7.68
7.66
7.52
7.49
7.47
7.38
7.35
7.33
4.83
4.58
3.85
3.37
3.32
3.29
3.04
2.51
2.51
2.50
2.50
2.49
2.08
2.00
1.06
4.08
3.91
2.03
1.08
2.64
8.26
2.50
2.26

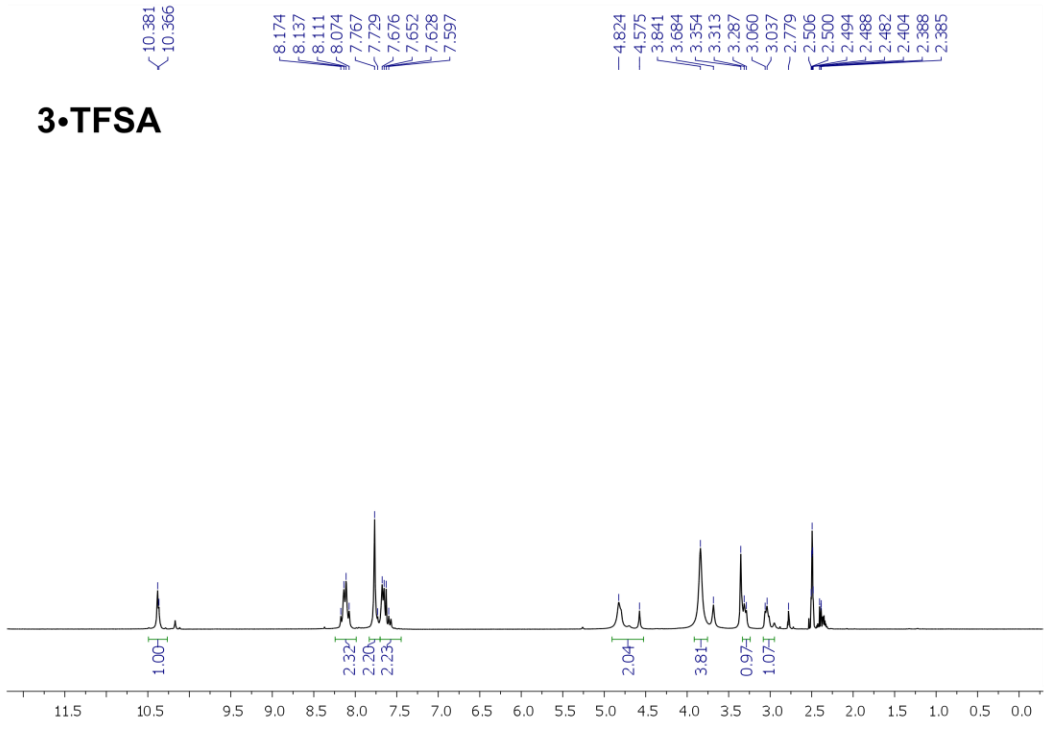
3•TFSA
10.381
10.366
8.174
8.137
8.111
8.074
7.767
7.729
7.676
7.652
7.628
7.597
4.824
4.575
3.841
3.684
3.354
3.313
3.287
3.060
3.037
2.779
2.506
2.500
2.494
2.488
2.482
2.404
2.388
2.385
1.00
2.32
2.20
2.23
2.04
3.81
0.97
1.07

Figure S3. ^{1}H-NMR (300 MHz) spectra of ionenes (**1**–**3**)·**TFSA** in DMSO-d_6.

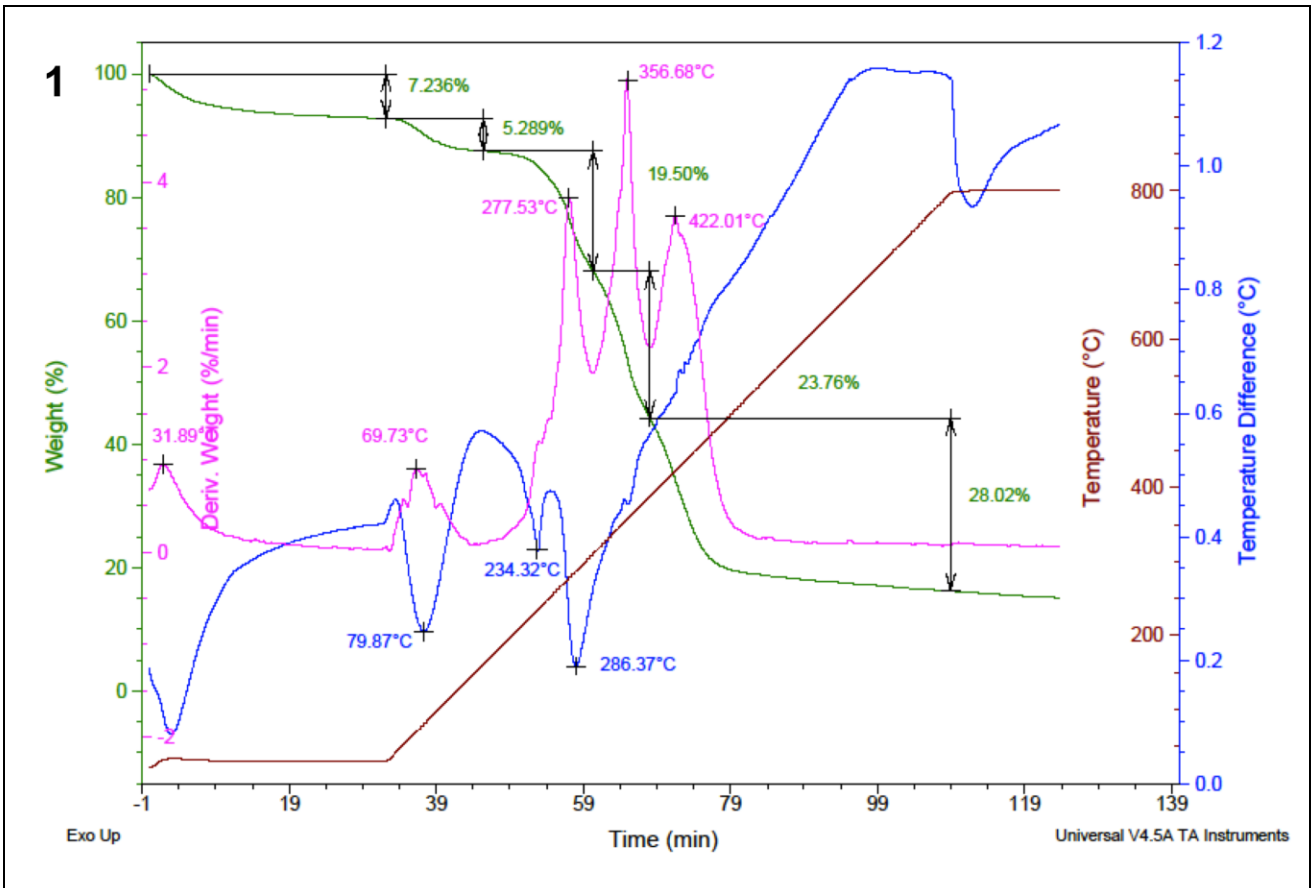
1
Weight (%)
Deriv. Weight (%/min)
Temperature (°C)
Temperature Difference (°C)
Time (min)
Exo Up
Universal V4.5A TA Instruments
7.236%
5.289%
19.50%
23.76%
28.02%
356.68°C
277.53°C
422.01°C
31.89°C
69.73°C
234.32°C
79.87°C
286.37°C

2

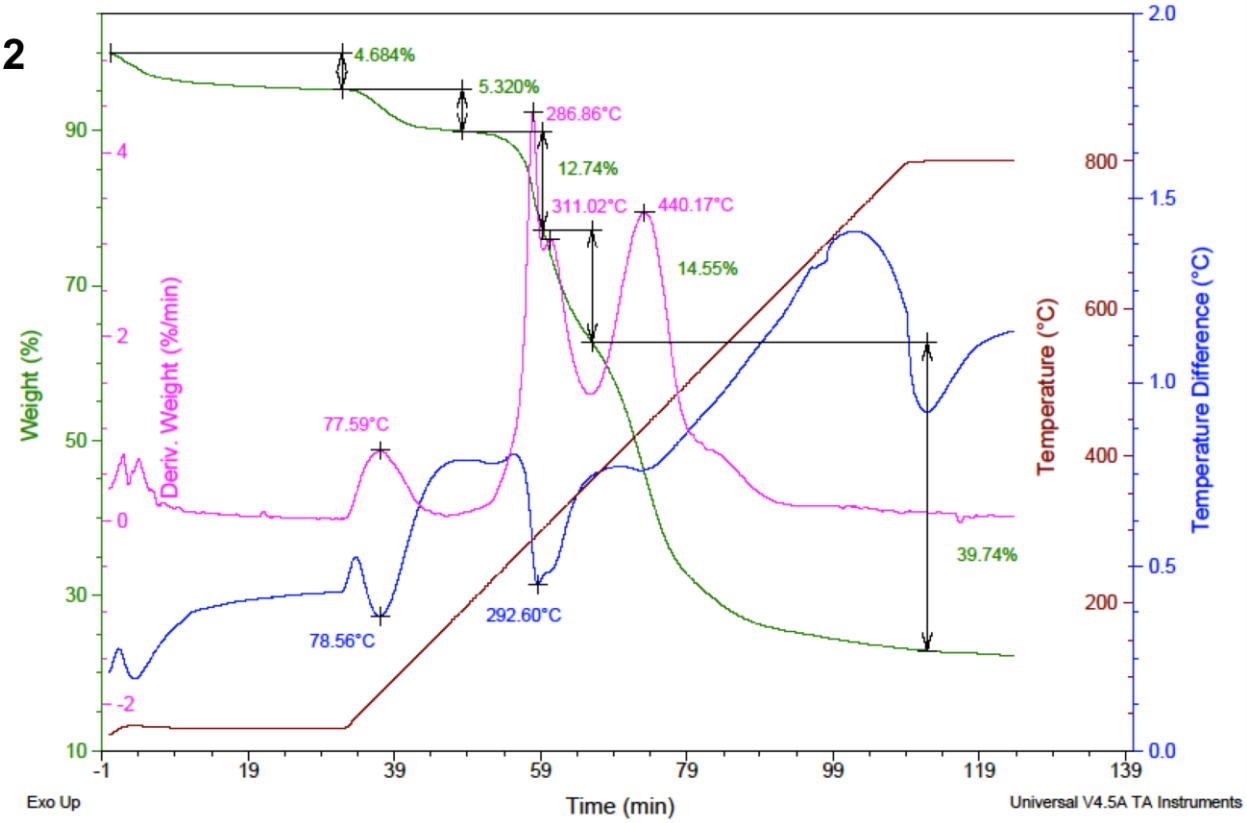
4.684%
5.320%
286.86°C
12.74%
311.02°C
440.17°C
14.55%
77.59°C
78.56°C
292.60°C
39.74%
Weight (%)
Deriv. Weight (%/min)
Temperature (°C)
Temperature Difference (°C)
Time (min)
Exo Up
Universal V4.5A TA Instruments

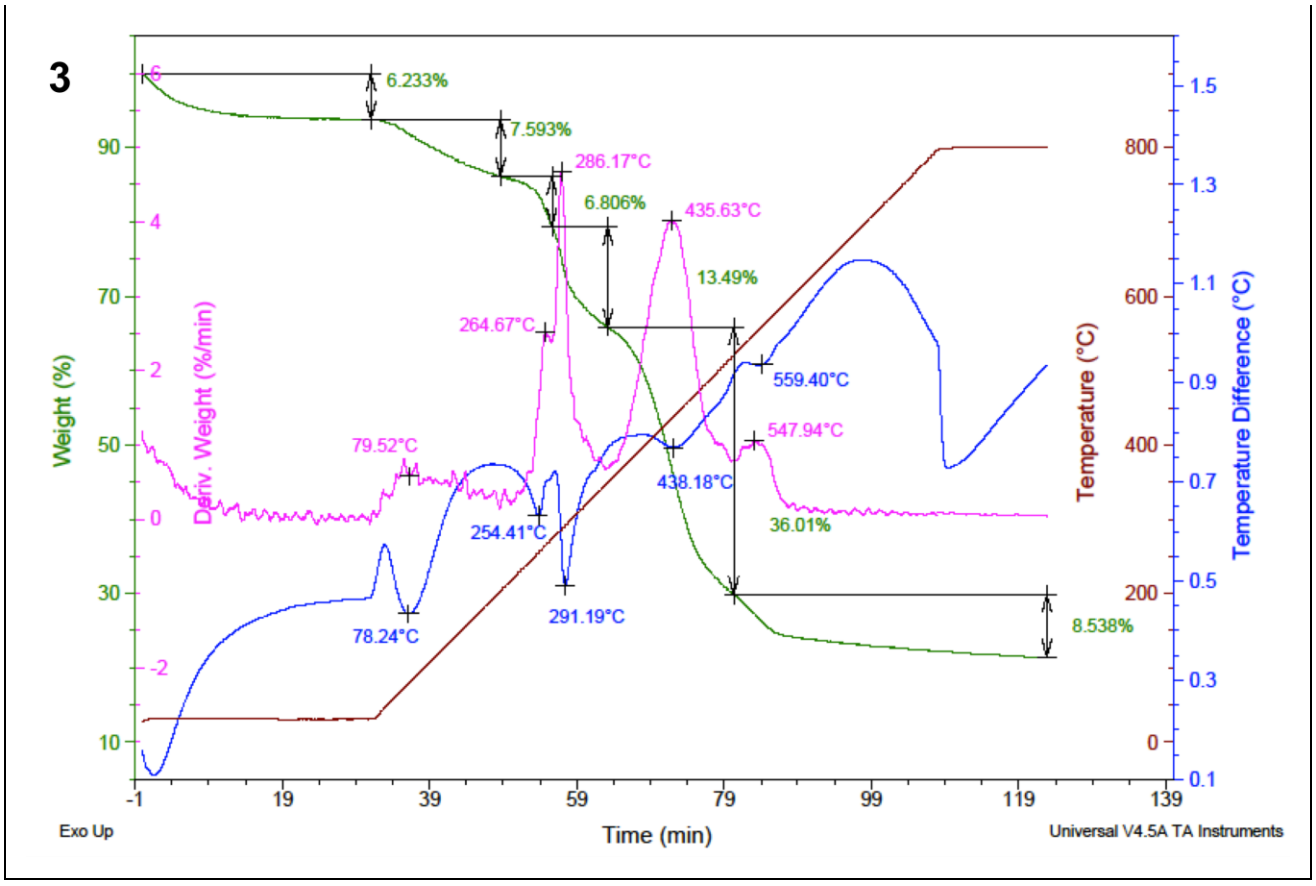

Figure S4. ATD/ DSC/ TGA spectra of ionenes **1**–**3**.

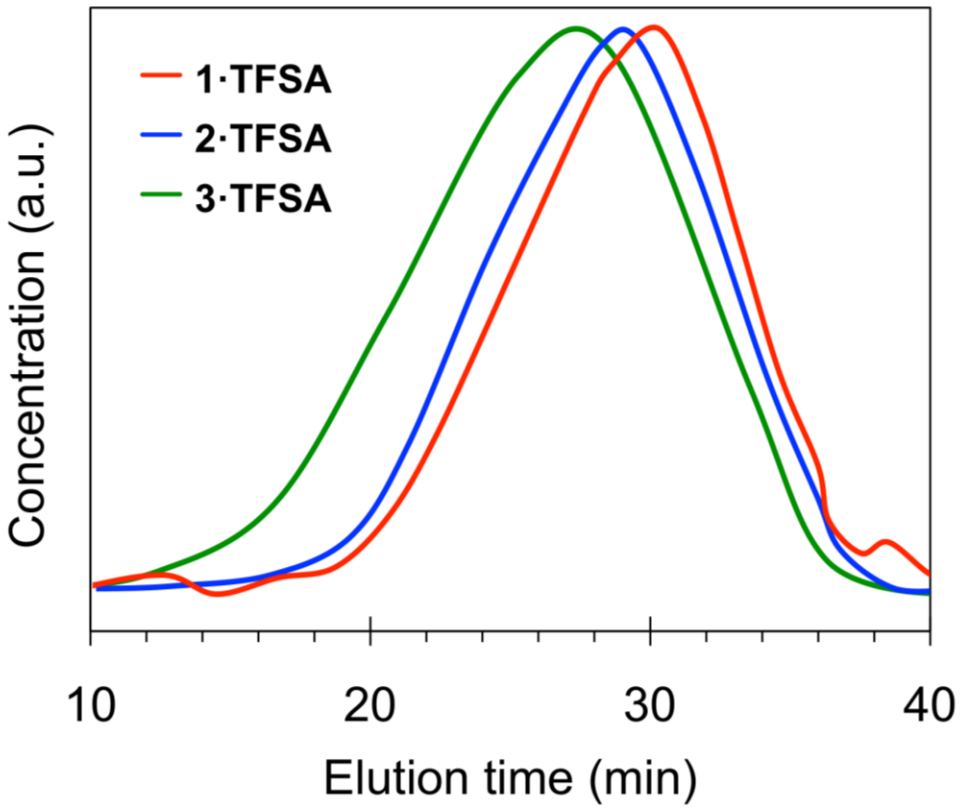

Figure S5. SEC traces of **1·TFSA** (M_w = 9.1 × 10^3 Da; M_n = 9.1 × 10^3 Da; $Đ_M$ = 2.1; n =7), **2·TFSA** (M_w = 1.2 × 10^4 Da; M_n = 9.1 × 10^3 Da; $Đ_M$ = 2.4; n =7), **3·TFSA** (M_w = 1.7 × 10^4 Da; M_n = 9.1 × 10^3 Da; $Đ_M$ = 2.9; n =10).

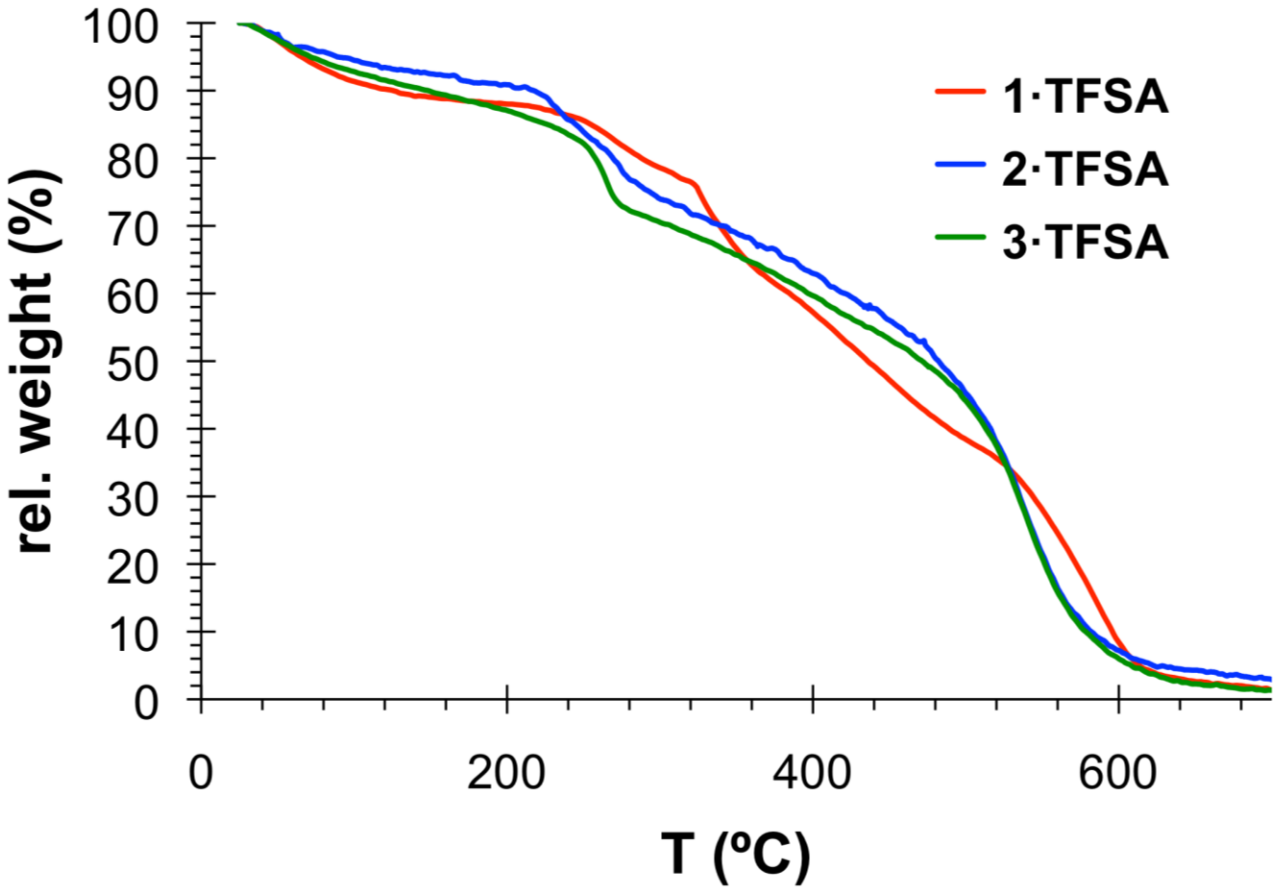

Figure S6. TGA analyses of ionenes (**1**–**3**)·**TFSA**.

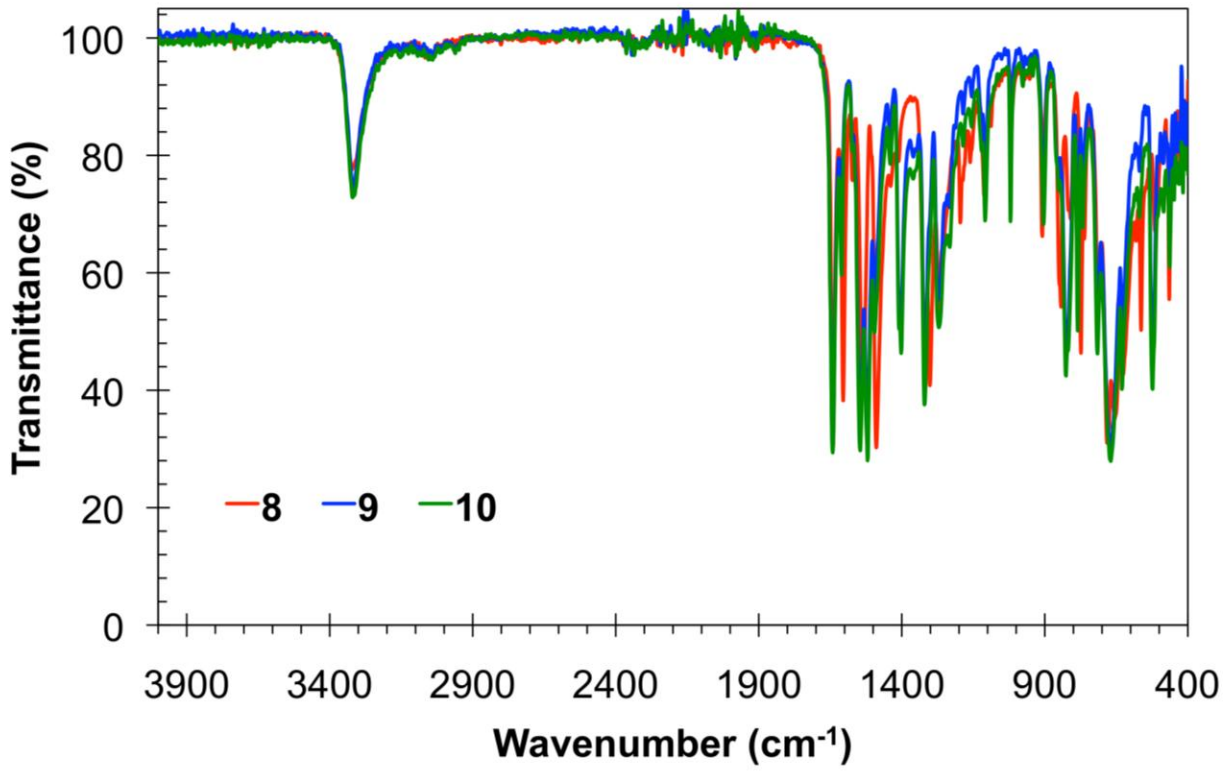
100
80
60
40
20
0
Transmittance (%)
8
9
10
3900
3400
2900
2400
1900
1400
900
400
Wavenumber (cm-1)

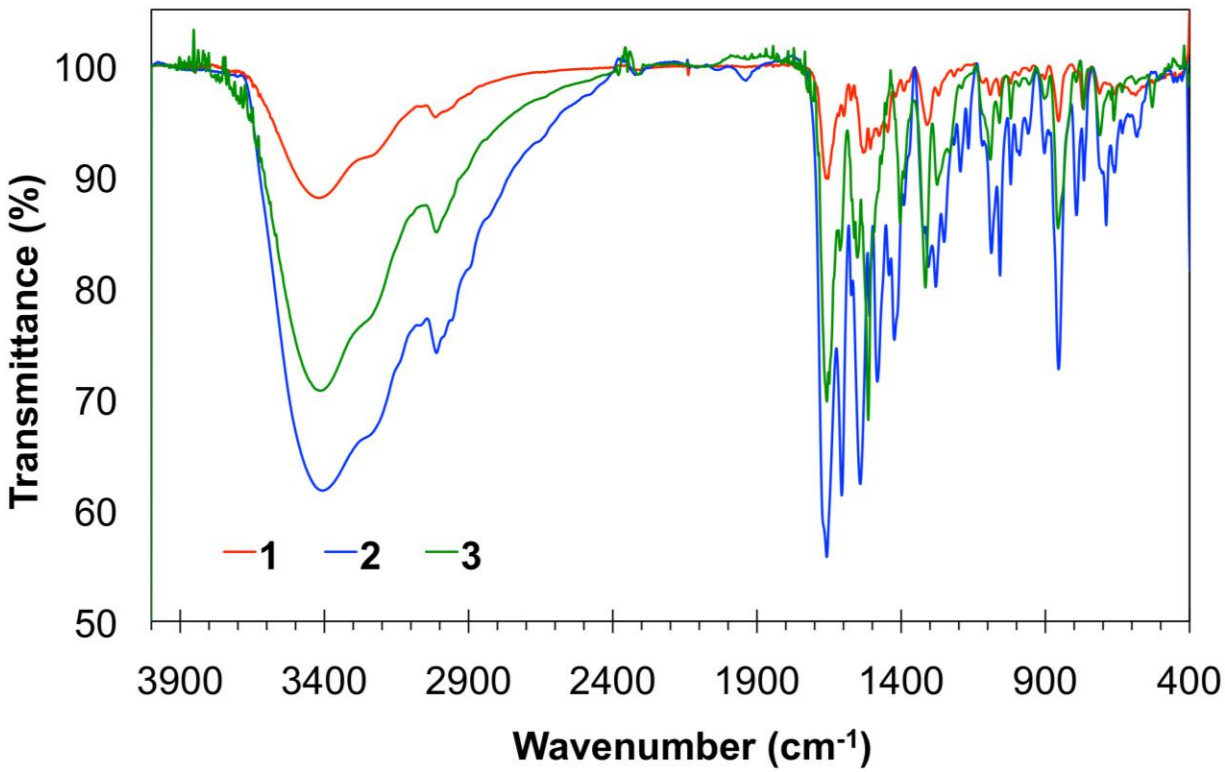
100
90
80
70
60
50
Transmittance (%)
1
2
3
3900
3400
2900
2400
1900
1400
900
400
Wavenumber (cm-1)

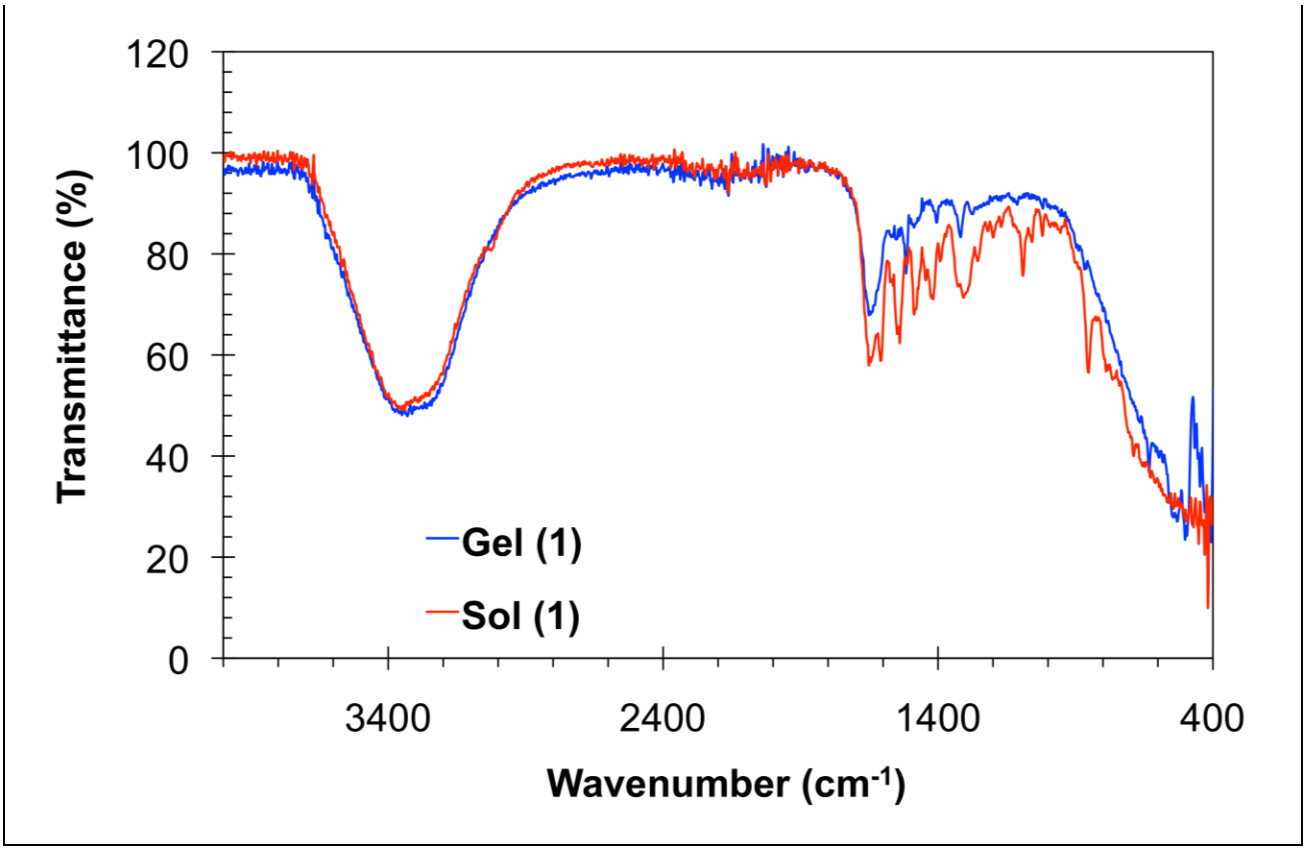

Figure S7. FT-IR spectra of precursors **8**–**10**, ionenes **1**–**3**, and comparison between gel phase and solution phase in the case of **1**.

Table S2. Comparative properties of hydrogels made of **1**, **2** and **3**.

Ionene	CGC (g L^{-1})	Optical appearance	Gelation time	T_{gel} (°C)
1	25 ± 2.0	transparent gel	4 ± 0.2 min	64 ± 1
2	100 ± 10.0	white-opaque gel	20 ± 0.5 h	59 ± 1
3	48 ± 5.0	white-opaque gel	77 ± 5 min	58 ± 1

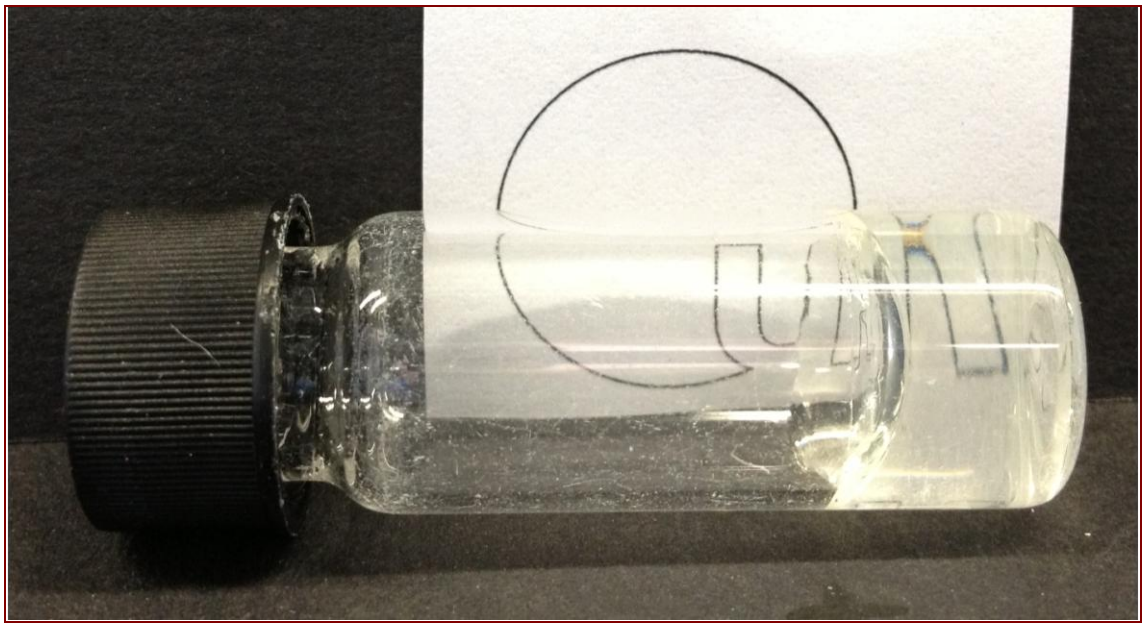

Figure S8. Digital photograph of the transparent hydrogel obtained from **1** (c = 25 g L^{-1} = CGC).

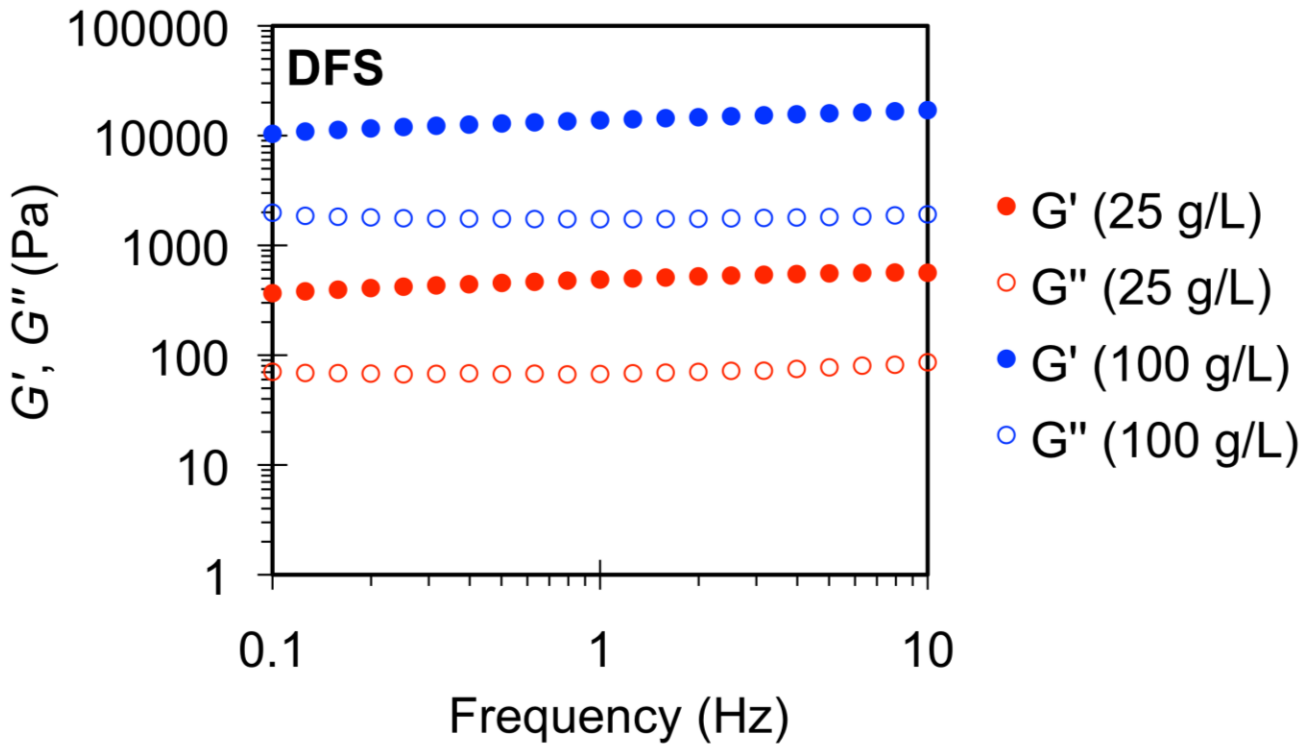

Figure S9. Effect of the gelator concentration on the mechanical properties of the material made of **1**. For c = 25 g L^{-1}: G' = 510 ± 95.5 Pa; tan δ = 0.14 ± 0.023. For c = 100 g L^{-1}: G' = 13938 ± 2644.3 Pa; tan δ = 0.11 ± 0.001.

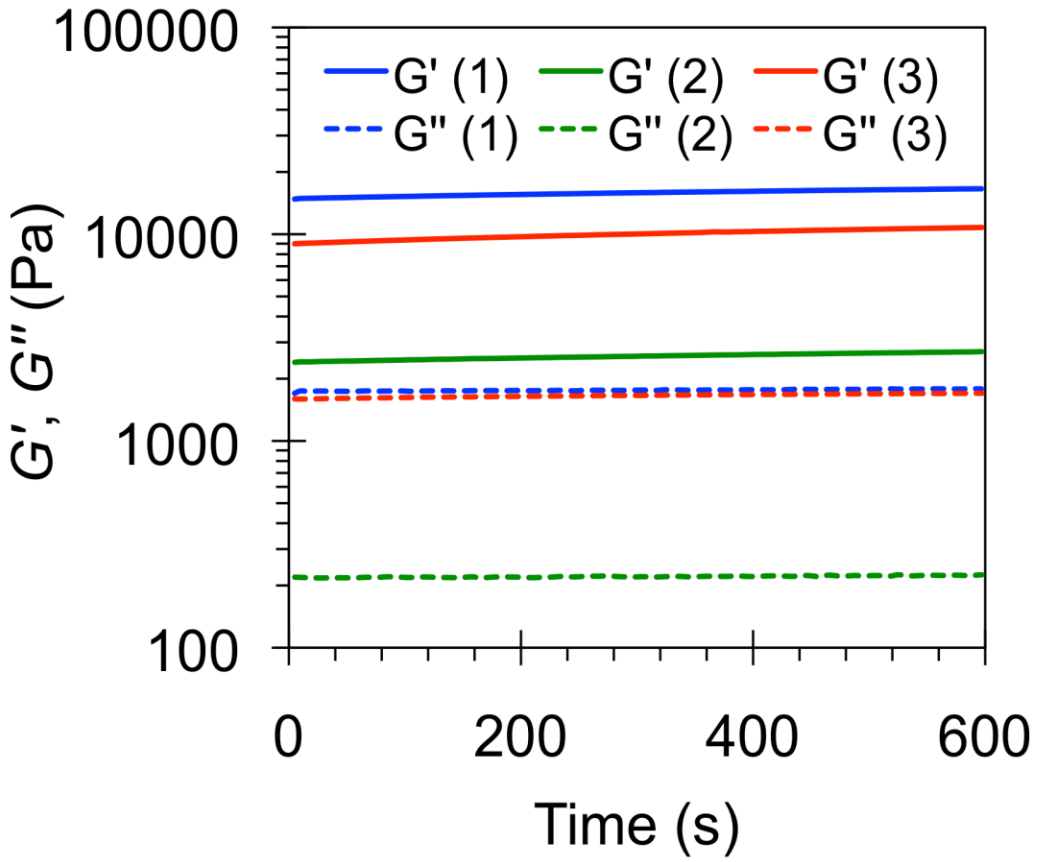

Figure S10. DTS rheological experiments of hydrogels made from **1**, **2** or **3** at their CGC. Average values obtained from two independent runs, for **1**: G' = 510 ± 95.5 Pa; tan δ = 0.14 ± 0.023; for **2**: G' = 2522 ± 102.5 Pa; tan δ = 0.09 ± 0.02; for **3**: G' = 218 ± 27.4 Pa; tan δ = 0.17 ± 0.008.

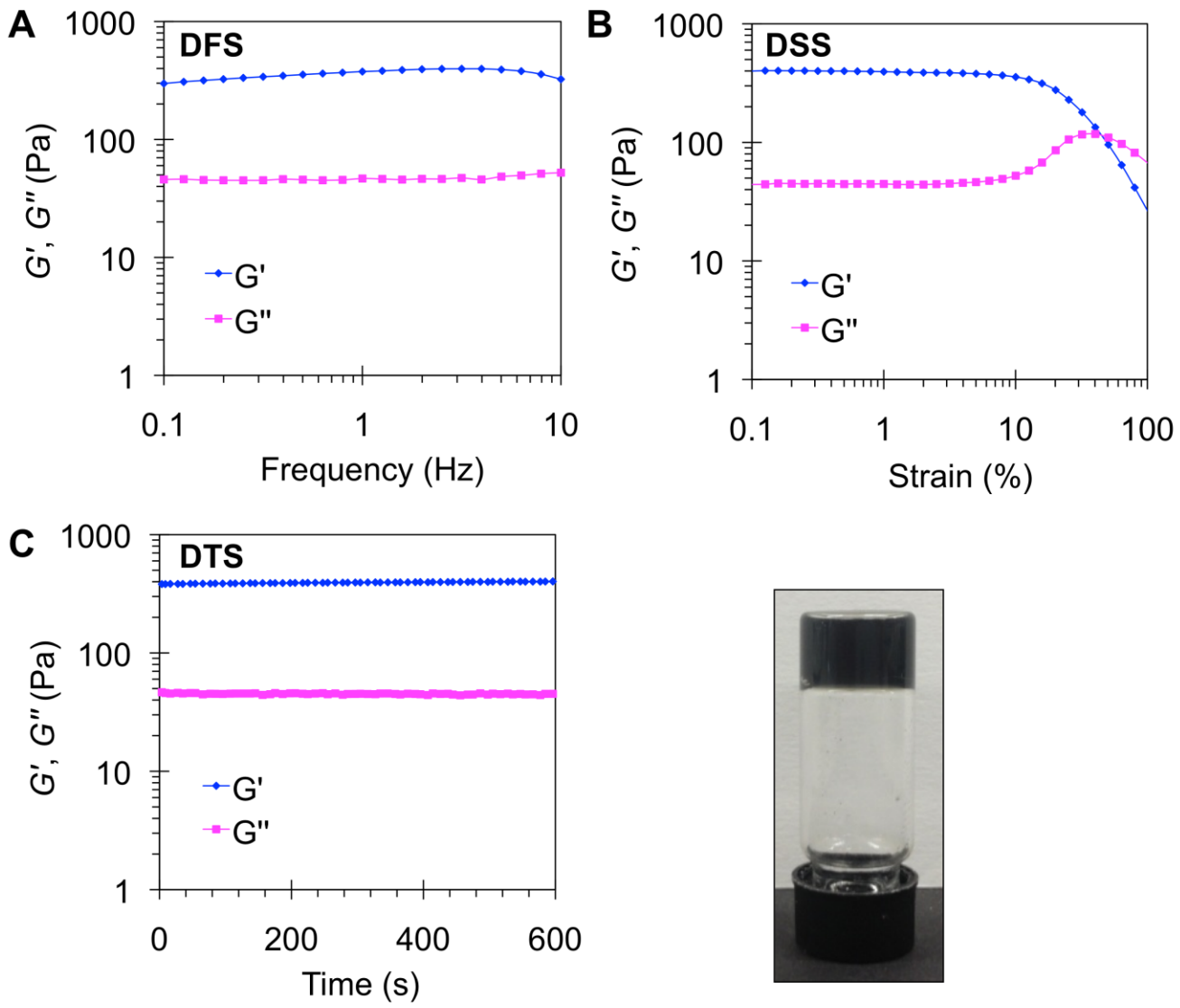

Figure S11. Oscillatory rheological characterization of hydrogel composite made from **1** (c = 25 g L^{-1}) and SWNTs (c = 0.1 g L^{-1}) at 25 ºC. The tan δ values for the pristine and composite hydrogels were 0.14 ± 0.02.

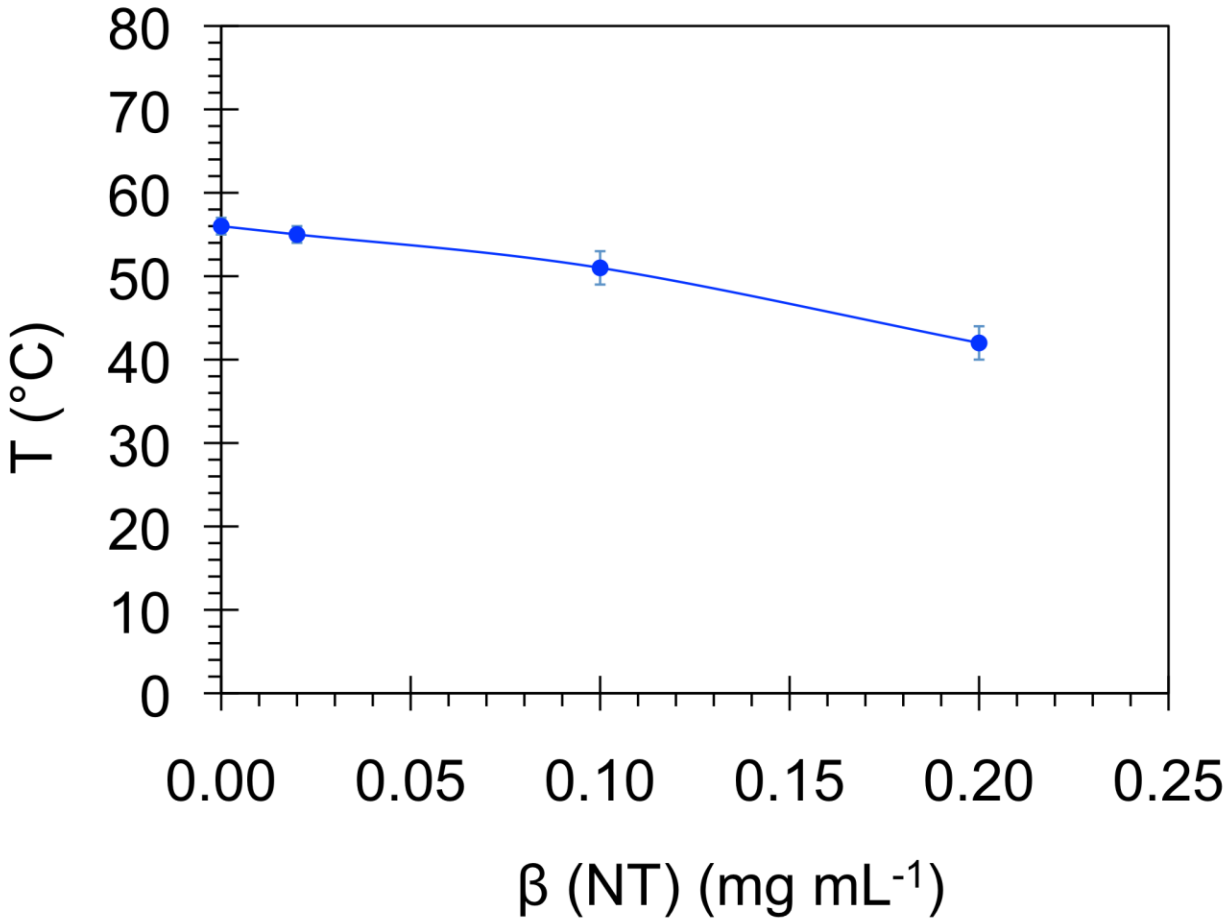

Figure S12. Effect on the T_{gel} of the hydrogel made from **1** (c = 25 g L^{-1}) upon incorporation of increasing concentration of SWNTs.

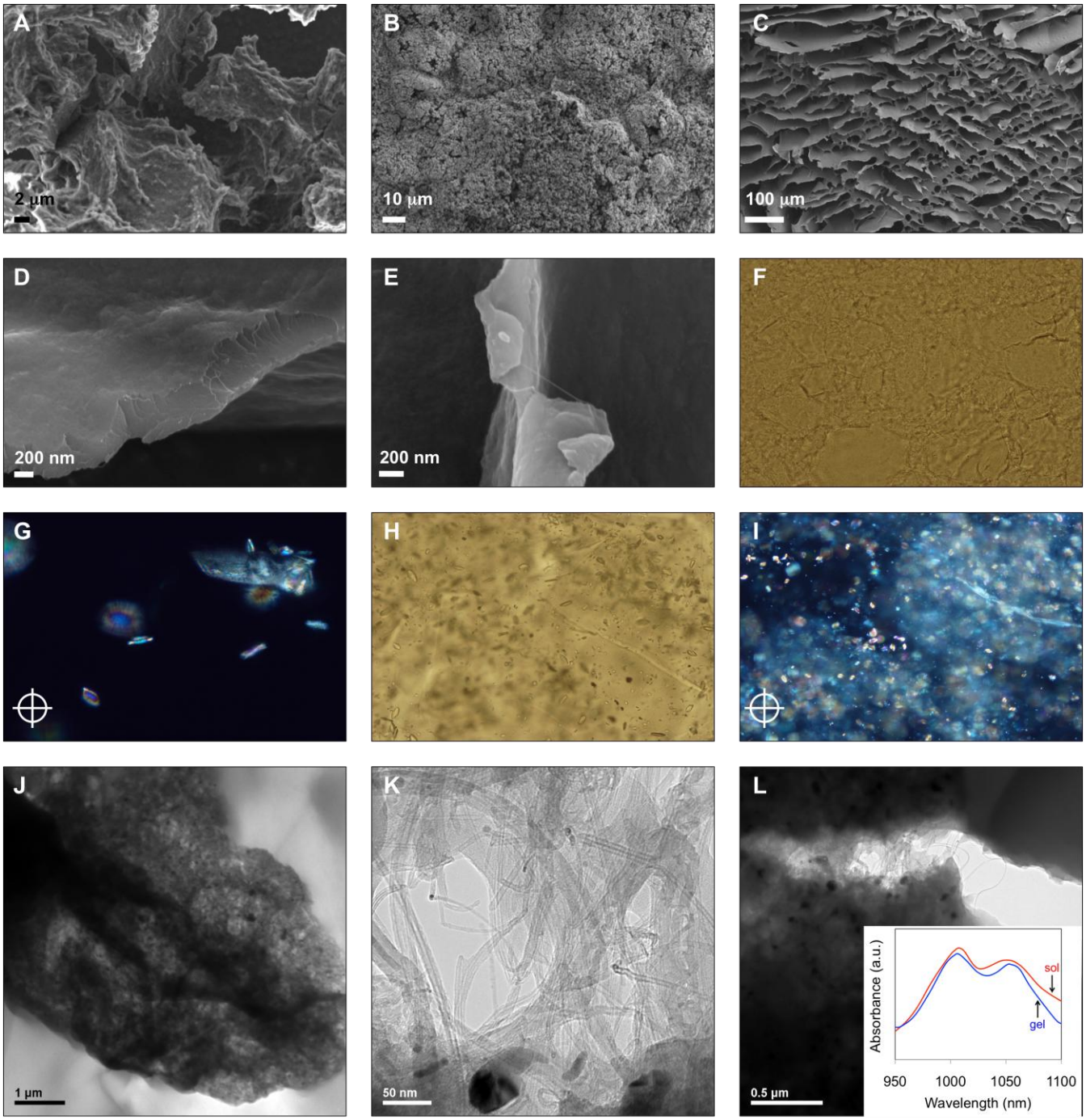

Figure S13. Additional FE-SEM; TEM and optical images (OI): A) FE-SEM image of the xerogel derived from **1** (c = 50 g L^{-1}); B) FE-SEM image of the xerogel derived from **2** (c = 100 g L^{-1}); C) FE-SEM image of the xerogel derived from **3** (c = 100 g L^{-1}); D-E) FE-SEM image of the xerogel derived from **1** (c = 25 g L^{-1}) containing SWNTs (c = 0.1 g L^{-1}); F) OI (20×) of the hydrogel film made of **1** (c = 100 g L^{-1}); G) OI (50×) of the hydrogel film made of **1** (c = 25 g L^{-1}) under crossed nicols; H) OI (20×) of the hydrogel film made of **1** (c = 25 g L^{-1}) containing SWNTs (c = 0.1 g L^{-1}); I) OI (10×) of the hydrogel film made of **1** (c = 25 g L^{-1}) containing SWNTs (c = 0.1 g L^{-1}) under crossed nicols; J-L)

TEM images of the xerogel derived from **1** (c = 25 g L^{-1}) containing SWNTs (c = 0.1 g L^{-1}) at different magnifications. Inset: Corresponding Vis-NIR spectra of both sol and gel phases.

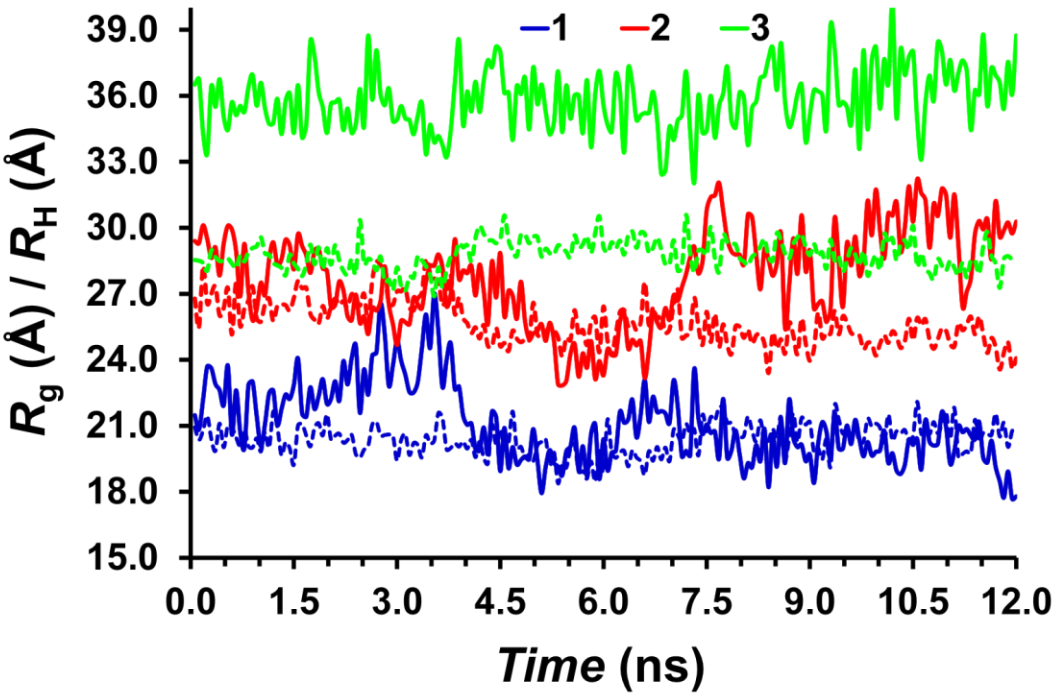

Figure S14. Temporal evolution of the radius of gyration (R_g) and hydrodynamic radius (R_H), which are represented by solid and dashed lines, respectively, obtained for **1**, **2** and **3**.

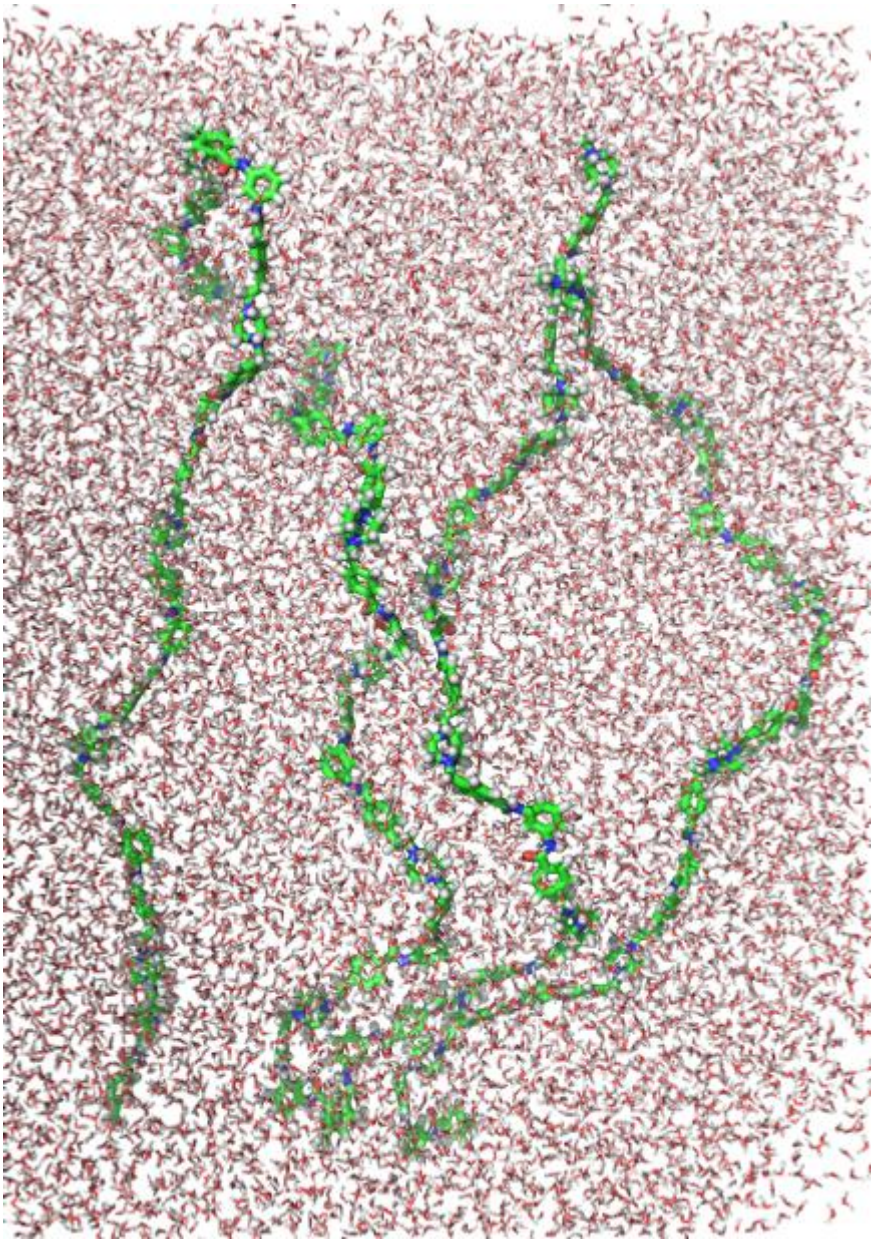

Figure S15. Representative snapshot taken from simulations on model **2e**, which consists of four explicit polymer chains with n = 6 each one immersed in a simulation box filled with 98498 explicit water molecules.

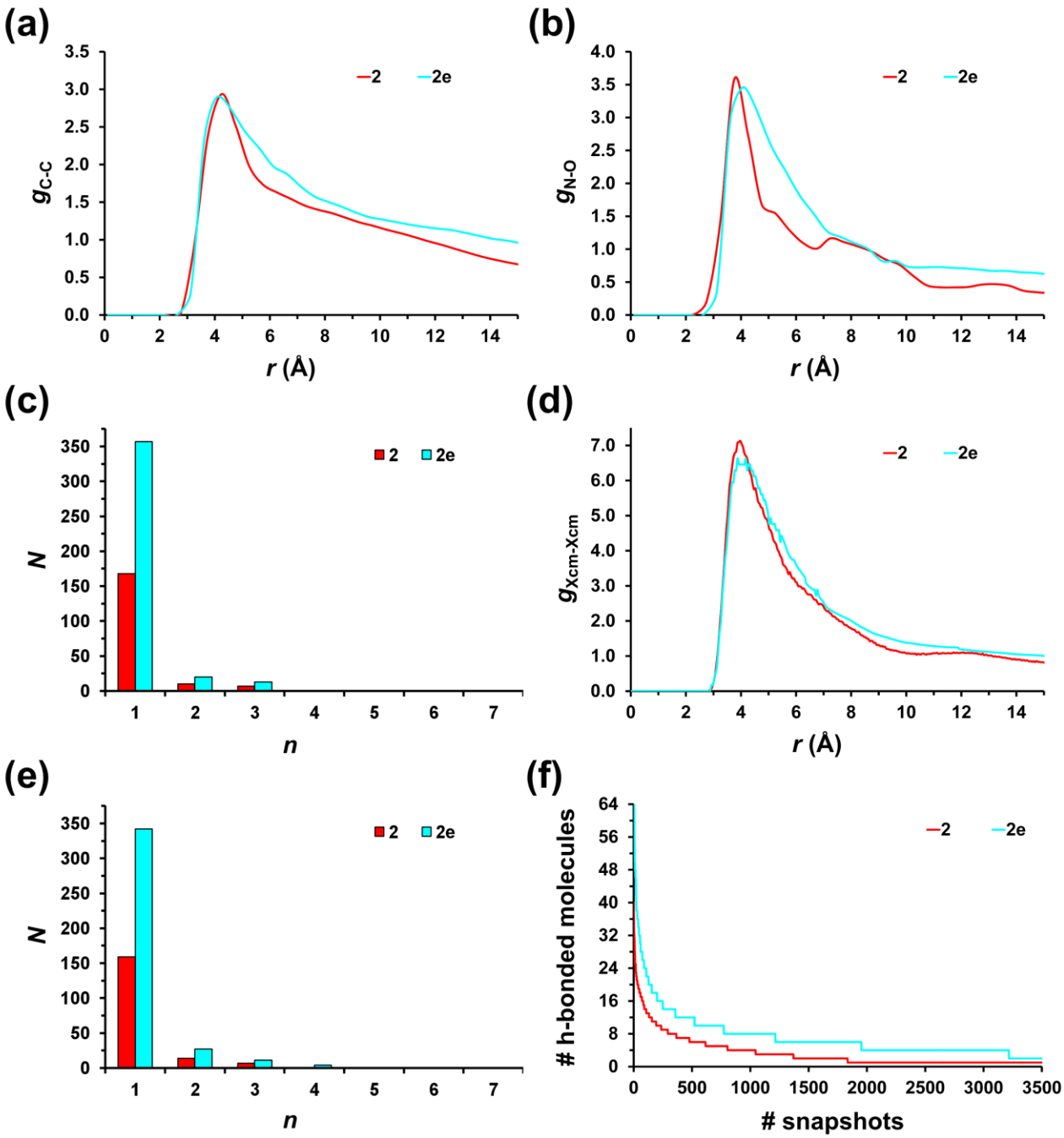

Figure S16. Radial distribution functions for the (a) C···C and (b) N···O pairs of atoms belonging to different ionene polymer chains for **2** and **2e**. (c) Number of N···O hydrogen bonds (*N*) with life times comprised between 0 and 0.5 ns (*n* = 1), 0.5 and 1.0 ns (*n* = 2) and 1.0 and 1.5 ns (*n* = 3). (d) Radial distribution functions for pairs of centers of masses of aromatic rings belonging to different ionene polymer chains for **2** and **2e**. (e) Number of π-π stacking interactions (*N*) with life times comprised between 0 and 0.5 ns (*n* = 1), 0.5 and 1.0 ns (*n* = 2), 1.0 and 1.5 ns (*n* = 3) and 1.5 and 2.0 ns (*n*= 4). (f) Number of water molecules involved in hydrogen bonding interactions with the amide groups of the

polymer chains in **2** and **2e** against the number of snapshots. A decreasing order is displayed for the three evaluated systems. The radial distribution functions displayed in (a), (b) and (e) have been normalized for comparison between the two systems.

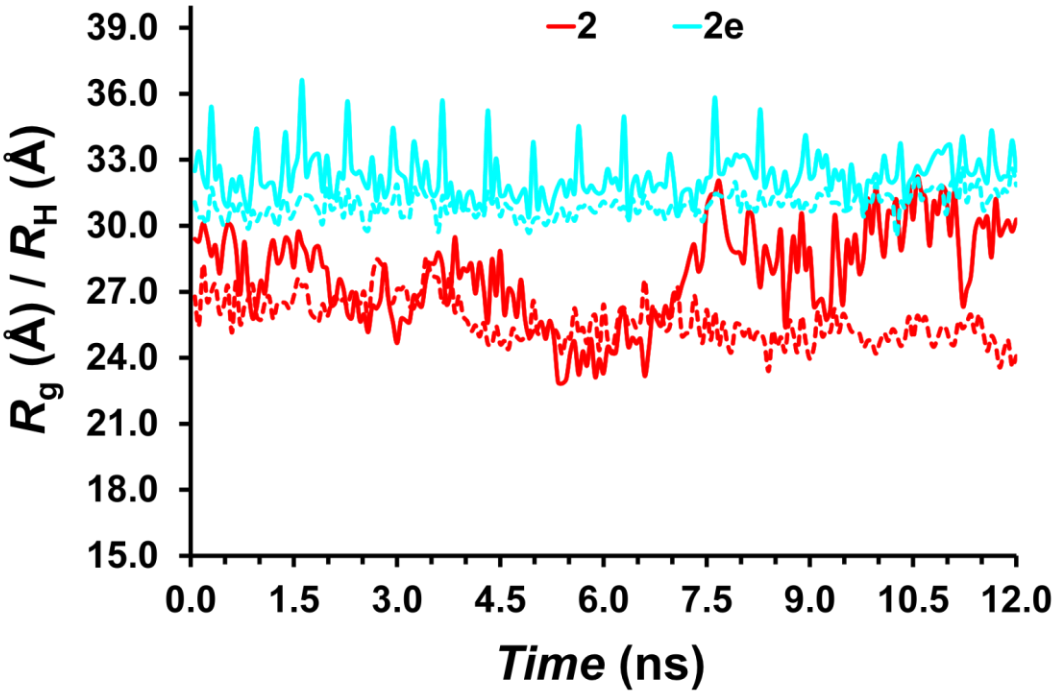

Figure S17. Temporal evolution of the radius of gyration (R_g) and hydrodynamic radius (R_H), which are represented by solid and dashed lines, respectively, obtained for **2** and **2e**.

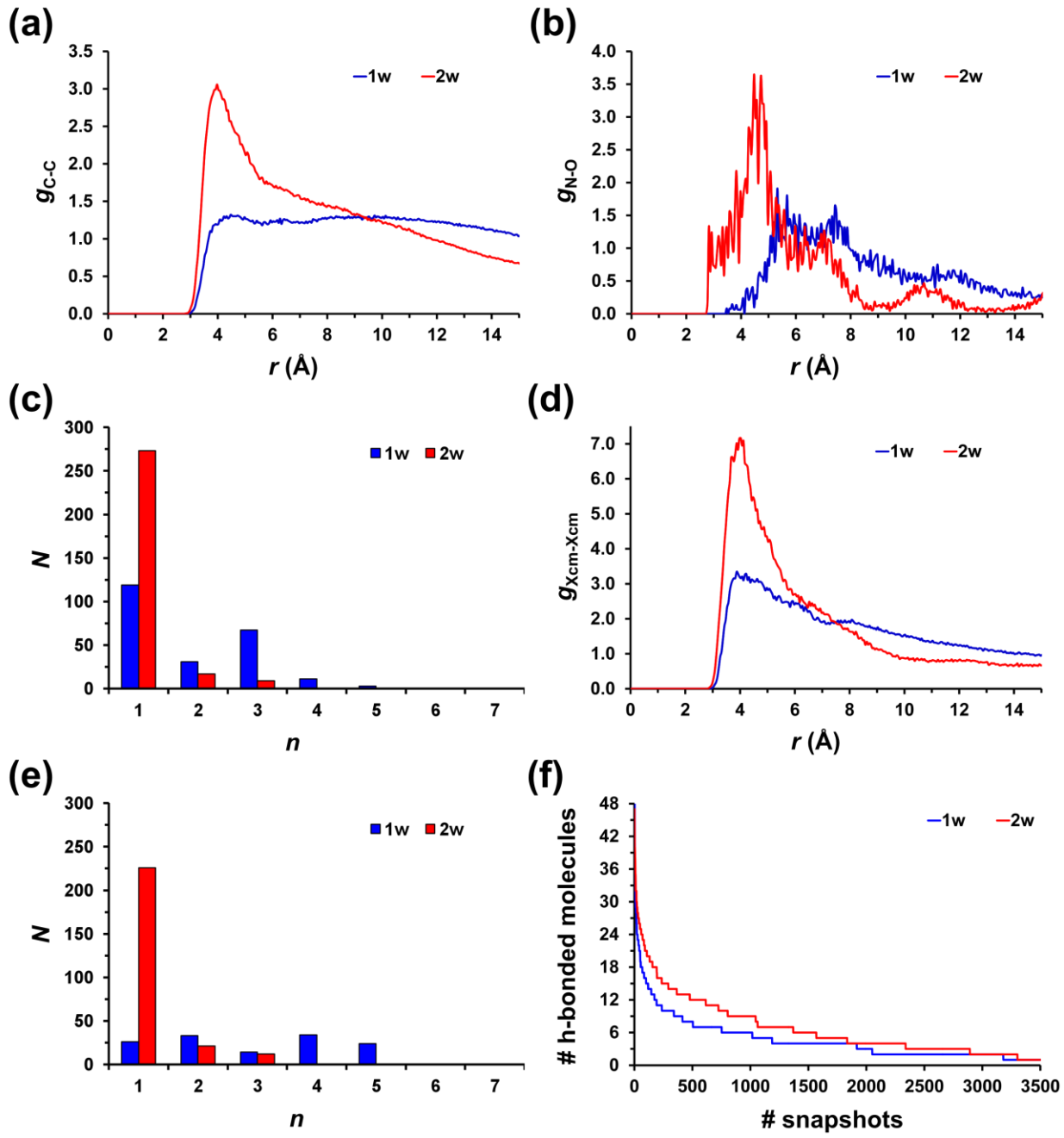

Figure S18. Radial distribution functions for the (a) C···C and (b) N···O pairs of atoms belonging to different ionene polymer chains for **1w** and **2w**. (c) Number of N···O hydrogen bonds (*N*) with life times comprised between 0 and 0.5 ns (*n* = 1), 0.5 and 1.0 ns (*n* =2), 1.0 and 1.5 ns (*n* = 3), 1.5 and 2.0 ns (*n*= 4) and 2.0 and 2.5 ns (*n*= 5). (d) Radial distribution functions for pairs of centers of masses of aromatic rings belonging to different ionene polymer chains for **1w** and **2w**. (e) Number of π-π stacking interactions (*N*) with life times comprised between 0 and 0.5 ns (*n* = 1), 0.5 and 1.0 ns (*n* = 2), 1.0 and 1.5 ns (*n* = 3), 1.5 and 2.0 ns (*n* = 4) and 2.0 and 2.5 ns (*n* = 5). (f) Number of water molecules involved in hydrogen bonding interactions with the amide groups of the polymer chains in **1w** and **2w** against the

number of snapshots. A decreasing order is displayed for the three evaluated systems. The radial distribution functions displayed in (a), (b) and (d) have been normalized for comparison between the two systems.

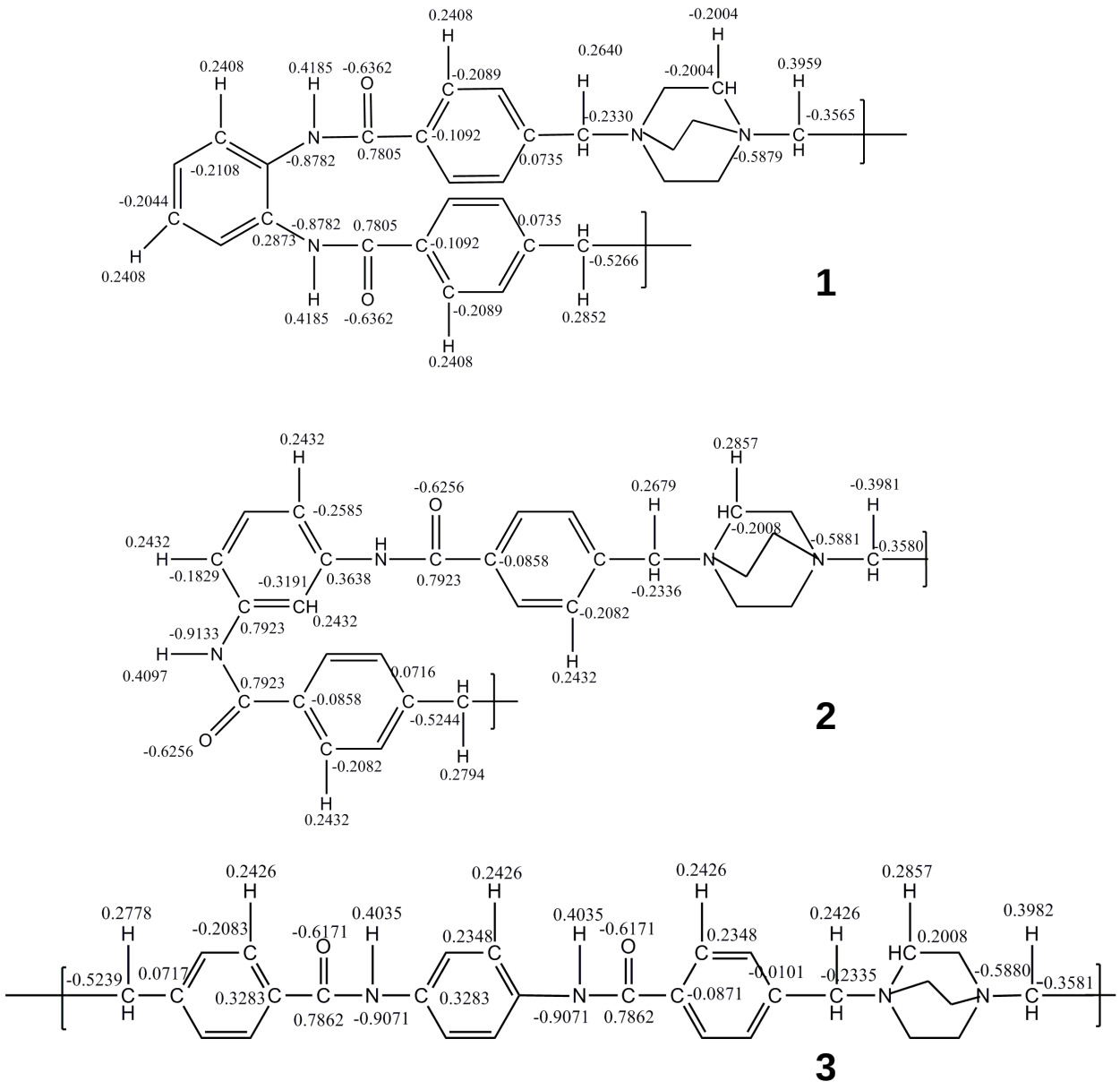

Figure S19. Electrostatic parameters for the repeat units of **1**, **2** and **3**.

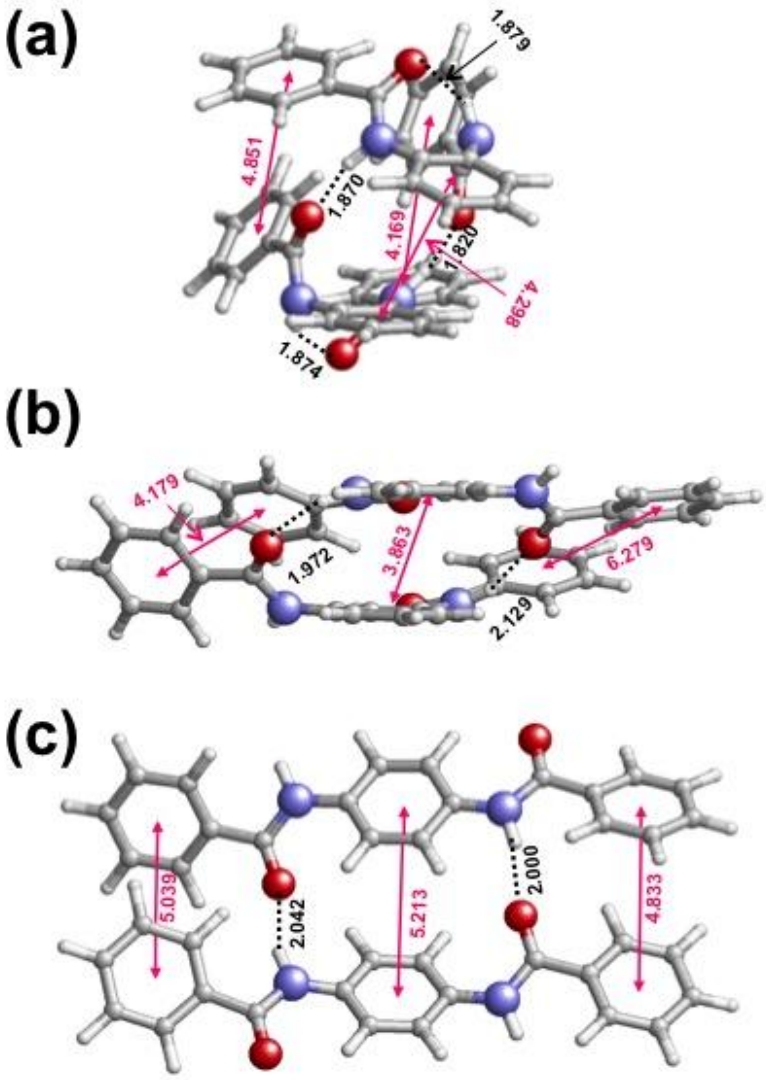

Figure S20. Geometries optimized at the M06L/6-31+G(d,p) level of model complexes calculated for (a) **1**, (b) **2** and (c) **3**. Intra- and intermolecular hydrogen bonds are indicuated using dashed lines (black) while π-π staking interactions are represented using arrows (pink). H···O distances for hydrogen bonds and distance between the centers of masses between the two rings are indicated for hydrogen bonds and π-π staking interactions (both in Å)

6. References

---

[i] M.T. Sierra (CSIC, Zaragoza), M. Piñol (Univ. Zaragoza), I. Osante (Univ. Zaragoza), C. Pobes (CSIC, Zaragoza), J.J. Marrero-Tellado (Univ. La Laguna), C.J. Hawker (UCSB, US), and J.A. Johnson (MIT, US) are also acknowledged for assistance with some measurements and/or useful discussions.

[ii] Wu, C. Handbook of Size Exclusion Chromatography; Marcel Dekker: New York, **1995**.

[iii] Takahashi, A.; Sakai, M.; Kato, T. *Polym. J.* **1980**, *12*, 335-341.

[iv] Jeong, S. W.; Shinkai, S. *Nanotechnology* **1997**, *8*, 179-183.

[v] Bachl, J.; Diaz, D. D. *Molbank* **2010**, *2010*, M705.

[vi] Yoshida, M.; Ohyama, H.; Matsuzawa, Y. PCT Int. Appl. (2011), WO 2011052601 A1 20110505.

[vii] Misawa, Y.; Koumura, N.; Matsumoto, H.; Tamaoki, N.; Yoshida, M. *Macromolecules* **2008**, *41*, 8841-8846.

[viii] Noguchi, H.; Rembaum, A. *Macromolecules* **1972**, *5*, 261-269, and references therein.

[ix] Misawa, Y.; Koumura, N.; Matsumoto, H.; Tamaoki, N.; Yoshida, M. *Macromolecules* **2008**, *41*, 8841-8846.

[x] Duan, Y.; Wu. C.; Chowdhury. S.; Lee, M. C.; Xiong. G.; Zhang, W.; Yang, R.; Cieplak, P.; Luo, R.; Lee, T.; Caldwell, J.; Wang, J.; Kollman, P. *J. Comput. Chem.* **2003**, *24*, 1999-2012.

[xi] Jorgensen, W. L.; Chandrasekhar, J.; Madura, J. D.; Impey, R. W.; Klein, M. L. *J. Chem. Phys.* **1983**, *79*, 926-935.

[xii] Toukmaji, A.; Sagui, C.; Board, J.; Darden, T. *J. Chem. Phys.* **2000**, *113*, 10913-10927.

[xiii] Ryckaert, J. P.; Ciccotti, G.; Berendsen, H. J. C. *J. Comput. Phys.* **1977**, *23*, 327-341.

[xiv] Cornell, W. D.; Cieplak, P.; Bayly, C. I.; Gould, I. R.; Merz, K. M., Jr.; Ferguson, D. M.; Spellmeyer, D. C.; Fox, T.; Caldwell, J. W.; Kollman, P. A. *J. Am. Chem. Soc.* **1995**, *117*, 5179-5197.

[xv] Gaussian 03, Revision B.02, Frisch, M. J.; Trucks, G. W.; Schlegel, H. B.; Scuseria, G. E.; Robb, M. A.; Cheeseman, J. R.; Montgomery, J. A.; Vreven, T.; Jr., Kudin, K. N.; Burant, J. C.; Millam, J. M.; Iyengar, S. S.; Tomasi, J.; Barone, V.; Mennucci, B.; Cossi, M.; Scalmani, G.; Rega, N.; Petersson, G. A.; Nakatsuji, H.; Hada, M.; Ehara, M.; Toyota, K.; Fukuda, R.; Hasegawa, J.; Ishida, M.; Nakajima, T.; Honda, Y.; Kitao, O.; Nakai, H.; Klene, M.; Li, X.; Knox, J. E.; Hratchian, H. P.; Cross, J. B.; Adamo, C.; Jaramillo, J.; Gomperts, R.; Stratmann, R. E.; Yazyev, O.; Austin, A. J.; Cammi, R.; Pomelli, C.; Ochterski, J. W.; Ayala, P. Y.; Morokuma, K.; Voth, G. A.; Salvador, P.; Dannenberg, J. J.; Zakrzewski, V. G.; Dapprich, S.; Daniels, A. D.; Strain, M. C.; Farkas, O.; Malick, D. K.; Rabuck, A. D.; Raghavachari, K.; Foresman, J. B.; Ortiz, J. V.; Cui, Q.; Baboul, A. G.; Clifford, S.; Cioslowski, J.; Stefanov, B. B.; Liu, G.; Liashenko, A.; Piskorz, P.; Komaromi, I.; Martin, R. L.; Fox, D. J.; Keith, T.; M. A. Al-Laham, Peng, C. Y.; Nanayakkara, A.; Challacombe, M.; Gill, P. M. W.; Johnson, B.; Chen, W.; Wong, M. W.; Gonzalez, C.; Pople, J. A., Gaussian, Inc.: Pittsburgh, PA, **2003**.

[xvi] Phillips, J. C.; Braun, R.; Wang, W.; Gumbart, J.; Tajkhorshid, E.; Villa, E.; Chipot, C.; Skeel, R. D.; Kale, L.; Schulten, K. *J. Comput. Chem.* **2005**, *26*, 1781-1802.

[xvii] Toxvaerd, S. *J. Chem. Phys.* **1990**, *93*, 4290-4295.

[xviii] Berendsen, H. J. C.; Postma, J. P. M.; van Gunsteren, W. F.; DiNola, A.; Haak, J. R. *J Chem Phys* **1984**, *81*, 3684-3690.

[xix] Martyna, G. J.; Tobia, D. L.; Klein, M. L. *J. Chem. Phys.* **1994**, *101*, 4177-4189.

[xx] Feller, S. E.; Zhang, Y.; Pastor, R. W.; Brooks, B. R. *J. Chem. Phys.* **1995**, *103*, 4613-4622.

[xxi]. Zhao, Y.; Truhlar, D. G. *J. Chem. Phys.* **2006**, *125*, 194101.

[xxii]. Hariharan, P. C.; Pople, J. A. *Theor. Chim. Acta* **1973**, *28*, 213-222.

[xxiii]. McLean, A. D.; Chandler, G. S. *J. Chem. Phys.* **1980**, *72*, 5639-5648.

[xxiv]. Remya, K.; Suresh, C. H. *J. Comput. Chem.* **2013**, *34*, 1341-1353.

[xxv]. Boys, S. F.; Bernardi, F. *Mol. Phys.* **1970**, *19*, 553-566.

[xxvi]. Tomasi, J.; Mennucci, B.; Cammi, R. *Chem. Rev.* **2005**, *105*, 2999-3094.